GEMTIP MODELING OF HETEROGENEOUS ROCK SAMPLES USING THE GENETIC ALGORITHMS

by

Wei Lin

A thesis submitted to the faculty of
The University of Utah
in partial fulfillment of the requirements for the degree of

Master of Science

in

Geophysics

Department of Geology and Geophysics

The University of Utah

December 2017

The University of Utah Graduate School

STATEMENT OF THESIS APPROVAL

The thesis of **Wei Lin**

has been approved by the following supervisory committee members:

Michael S. Zhdanov	, Chair	**03/22/2017** Date Approved
Erich U. Peterson	, Member	**05/01/2017** Date Approved
Alexander V. Gribenko	, Member	**05/01/2017** Date Approved

and by **Thure E. Cerling** , Chair of the Department of **Geology and Geophysics**

and by David B. Kieda, Dean of The Graduate School.

ABSTRACT

The generalized effective-medium theory of induced polarization (GEMTIP) provides fundamental equations, which describe in analytical form the relationships between the petrophysical parameters of the rocks and their complex resistivity (CR) as a function of frequency. These relationships can be used to determine the petrophysical properties of the rocks from the observed CR data. However, for the three-phase ellipsoidal GEMTIP model, the inversion of the CR data has proven to be very challenging due to nonuniqueness and instability of this problem. In a number of practical situations, the gradient-type methods may experience significant difficulties due to existence of many local minima in the search space. In this thesis, the inversion methods for the GEMTIP modeling of heterogeneous rock samples are developed based on the genetic algorithms.

I have conducted the synthetic study to prove that the pure genetic algorithm can be used for the GEMTIP inversion. However, it is showed that this method is not an ideal solution. To improve the inversion method, a hybrid adaptive genetic algorithm with simulated annealing (SAAGA) for the GEMTIP inversion was developed. The synthetic study demonstrated that this method provided an effective solution for the GEMTIP inverse problems and made it possible to find the global minimum in the space of GEMTIP model parameters. The case study included interpretation of the practical CR curves for different mineral rock samples. This case study demonstrated the advantage of

the developed method over the global minimum search (GMS) method and pure genetic algorithm with the SAAGA method. Finally, I have developed a modified hybrid genetic algorithm based on the SAAGA method and three-point crossover operation. The case study indicated that, by using the SAAGA with multipoint crossover operation the inversion results were significantly improved compared to the GMS method and SAAGA method.

To my wife Xinjie

CONTENTS

ACKNOWLEDGEMENTS

I would like to thank the Consortium for Electromagnetic Modeling and Inversion (CEMI) at the University of Utah for the financial and technical support. It provides an excellent environment for this research.

I also give my sincere thanks to my adviser and committee chair, Dr. Michael Zhdanov, for his expert guidance and support of my graduate study and research. I am also grateful for the inspiring classes that he taught on electromagnetic and inversion theory.

Thanks to Dr. Vladimir Burtman for helping my understanding of rock physics and providing the rock samples with the CR data, and thanks to Dr. Erich Petersen for providing the results from the QEMSCAN system. Special thanks go to Dr. Alex Gribenko for providing the GEMTIP forward modeling code and his valuable suggestions.

Finally, I would like to thank all those who helped me in the development of this project, and thank CEMI and TechnoImaging for providing the rock samples and the measurement of CR data. Especially, I thank my wife, Xinjie, for her moral support.

CHAPTER 1

INTRODUCTION

The induced polarization (IP) effect has found applications in mineral exploration (e.g., Pelton et al., 1978; Nelson, 1997) and in the search for oil and gas deposits (e.g., Vanhala, 1997). The IP effect is caused by complex frequency dependent distribution of the conductivities in the multiphase heterogeneous rock formations. Over the past decades, several different conductivity relaxation models were developed to study the complex resistivity (CR) of rocks, including the empirical Cole-Cole model (Cole and Cole, 1941; Pelton et al., 1978). This widely accepted empirical model describes the frequency dependence of CR reasonably well. However, it does not provide a direct relationship between the CR spectra and rock properties.

The generalized effective-medium theory of induced polarization (GEMTIP) was introduced recently in order to provide a link between the petro-physical properties of the rocks and their CR spectra (Zhdanov, 2008). GEMTIP uses effective-medium theory to describe the resistivity of the multiphase heterogeneous rocks and its relationship with the rocks' physical and electrical properties, including grain size, grain shape, porosity, polarizability, volume fraction, and conductivity of the inclusions (Zhdanov et al., 2009).

The GEMTIP model provides fundamental equations, which describe in analytical form the relationships between the petrophysical parameters of the rocks and their

complex resistivity. These equations can be used for studying the petrophysical characteristics of the rocks by analyzing the CR curves and inverting them for GEMTIP parameters. However, the inversion of the CR data proved to be very challenging due to nonuniqueness and instability of this problem. In a number of practical situations, the gradient-type methods may experience significant difficulties due to existence of many local minima in the search space (Gribenko, comm. pers.). In the past, the global minimum search (GMS) method was used to find the best solution with the given misfit condition and search intervals. However, this method is very time-consuming.

In this thesis, the global optimization techniques are applied to develop an effective approach for solving this problem. Chapter 2 presents the fundamental mechanism that causes the IP effect and describes the foundations of the GEMTIP theory. In Chapter 3, the pure genetic algorithm (GA) is first applied to the inversion. This method makes it possible to find the global minimum of GEMTIP inverse problem. However, the numerical tests shows that the GA inversion is unstable and the inversion results depend on the GA's parameters setting. In order to overcome this difficulty, the hybrid adaptive genetic algorithm with simulated annealing (SAAGA) for GEMTIP inversion has been developed. Compared to the GMS method and the GA, the SAAGA method provides an effective solution of GEMTIP inverse problem and converges rapidly to the global minimum for predicted data. However, in some rare circumstances, the observed CR curves of some rock samples are extremely complicated (e.g., weak local minimum of the CR curve). For these kinds of data, even the inversion result of the SAAGA method could not converge. To overcome this problem, I have developed a modified hybrid genetic algorithm based on the SAAGA method and multipoint crossover operation. Chapter 4 presents the case studies which demonstrate that by using

SAAGA with multipoint crossover operation the inversion results have been significantly improved compared to the GMS method and SAAGA method.

CHAPTER 2

EFFECTIVE MEDIUM THEORY OF COMPLEX RESISTIVITY

2.1 The Induced Polarization Effect

Generally there are two ways of presenting the IP effects. One way is based on examining the voltage as a function of frequency, which is known as frequency-domain IP effect. Another way is to measure the decay voltage as a function of time, which is called time-domain IP effect. Mathematically, the representations of the same IP phenomenon in the time or frequency domains are related (Kearey, 2009).

The IP effect is usually explained by the complex electrochemical processes in the rocks saturated with the water solutions. It is the result of (1) variations in the mobility of ions in fluids throughout the rock structure and (2) variations between ionic and electronic conductivity where metallic minerals are present (Telford et al., 1990). The first type of IP effect is called membrane polarization, which generally occurs in rocks that do not contain metallic minerals. The second one is known as the electrode polarization which is caused by mineral grains.

Figure 2.1 (a) shows the membrane polarization in a porous sandstone which is caused by a narrow pore channel. In some situations, the rock form minerals with a net negative charge on their outer surfaces, which are in contact with the pore fluid and

attract positive ions onto the inside surface. Those charges form a positively charged layer which is about 10^{-6} cm thick. If the diameter of the pore channel shrinks into less than this thickness, then the flow of ions will be blocked by the constriction when a voltage is applied. Thus, positive ions will increase their concentration while negative ions will leave the constricted zone, producing a potential difference across the blockage. After the applied voltage is switched off, the distribution of the ions will return to their original positions, which produces the measured IP response. This type of IP effect is known as membrane polarization (Telford, 1990).

When metallic minerals are present in a rock, the passage of the ions might be obstructed by the mineral grain. Figure 2.1 (b) shows a rock in which a metallic mineral grain blocks a pore space. When a voltage is applied, positive and negative charges are accumulated on the surface of the mineral grain, thus forming the electrical double layers. When the voltage is removed, the ions slowly return back to their original positions and cause a time delayed decaying voltage. This effect is known as the electrode polarization or overvoltage. Many rock containing minerals with good electric conductivity exhibit electrode polarization. These include rocks containing sulfides (e.g., pyrite, pyrrhotite, chalcopyrite, graphite, galena, and bornite), some oxides such as magnetite, etc. (Telford, 1990).

2.2 Methods of Measurement of IP Effect

As mentioned in the previous section, one can measure the induced polarization by observing the changes in voltage in time or frequency domains. The principles of these methods are similar, and are based on measuring the voltage between the electrodes as the observed data. However, they differ in a way of considering and measuring the signal

waveforms. Figure 2.2 (a) and (b) show the examples of measuring IP effect using the Wenner array in the time and frequency domain. For the time-domain IP method, the regular way is to send a direct current into the ground, and then record the decay of voltage between two electrodes after the cut-off of the current. On the contrary, the frequency-domain method usually uses two or more low frequencies alternating current (AC) to map the variation of apparent resistivity of the ground. Another frequency-domain method is called Complex Resistivity (CR) method. This method applies a current at frequency ranging from 0.001 Hz to 10 kHz into the ground and measures the amplitude of voltage as well as its phase with respect to the current. Generally, in the framework of the CR method one measures the real and quadrature components of the response, which can be transformed into amplitude and phase.

2.2.1 Time-Domain IP Method

In the direct current (DC) mode with the Wenner array, the voltage between the potential electrodes does not drop to zero immediately if the current is abruptly switched off. After a large initial decrease, the voltage decays gradually, as mentioned previously, and it takes some time to reach a zero value (Figure 2.3).

A similar phenomenon is observed as the current is switched on. The electric potential rises up immediately when the current is injected into the ground, but it takes several seconds to reach the steady state voltage value (maximum value). So the ground acts like a giant capacitor and becomes electrically polarized.

The length of time required for the overvoltage (V_s) to drop is recorded, and the time domain chargeability *m* is defined as the ratio between V_s and the steady state value of the potential (V_p):

$$m = \frac{V_s}{V_p}(mV/V). \tag{2.1}$$

However, due to electromagnetic conductive effects, it is difficult to measure V_s directly. The usual procedure is to measure the voltage at specific times (e.g., 0.5s) after cut-off and then measuring the decay of V_s within discrete intervals of time. The IP parameter in the time domain is the area under the decay curve of voltage $V_s(t)$ corresponding to the time interval (t_1, t_2). The integration of these values with respect to time gives the area under the curve (Figure 2.4), which is an alternative way of defining the chargeability. The resultant value of the integral divided by V_p is called the chargeability (m), which has the following expression:

$$m = \frac{\int_{t_1}^{t_2} V_s(t)\, dt}{V_p} = \frac{A}{V_p}, \tag{2.2}$$

where $V_s(t)$ is the off–time measured voltage at time t, V_p is the steady state value of the potential, and A is the area under the voltage decay curve between t_1 and t_2.

2.2.2 Frequency-Domain IP Method

IP effects can be also measured in the frequency domain. Using the Fourier transform, the frequency-domain IP method can be transformed from the time-domain method. In the frequency-domain measurement, the applied current is generally sampled at two frequencies (V_{low} and V_{high}) - each is at a decade apart and less than 10Hz (Zonge et al., 1971). Then the observed data of these frequencies can be used to explain the IP effect of the rocks. The derived parameter, frequency effect (FE), which is usually defined as:

$$\mathrm{FE} = \frac{V_{low} - V_{high}}{V_{high}}, \tag{2.3}$$

where V_{low} and V_{high} are the steady state voltage responses at the high and low frequencies, respectively. The equation (2.3) also can be written in the form of apparent resistivity:

$$\mathrm{FE} = \frac{\rho_2 - \rho_1}{\rho_1}, \tag{2.4}$$

where ρ_1 and ρ_2 are the apparent resistivity of the two frequencies respectively. Generally, the IP effect can be expressed by a percent frequency effect (PFE) as follows:

$$\mathrm{PFE} = \mathrm{FE} * 100\%. \tag{2.5}$$

2.2.3 Complex Resistivity (CR) Method

Another representation of IP effect in the frequency domain is the phase difference between the current in the source and the measured potential depending on multiple frequencies of the source (Figure 2.5), which is called complex resistivity (CR) method. The apparent resistivity is represented as a complex number as follows:

$$\rho_{\mathrm{a}}(\omega) = \rho_{\mathrm{real}}(\omega) + i\rho_{\mathrm{imag}}(\omega). \tag{2.6}$$

Using the Ohm's law, the amplitude and phase are defined as the difference in phase angle between the observed polarization voltage and the simulating current signal. The tangent of the phase angle is the ratio between the imaginary part and the real part of the observed polarization voltage (V_1 and V_2) or the complex resistivity (ρ_{real} and ρ_{imag}), which can be expressed as:

$$\phi = \tan^{-1}\frac{V_2}{V_1} = \tan^{-1}\frac{\rho_{\mathrm{imag}}}{\rho_{\mathrm{real}}}. \tag{2.7}$$

Generally, the voltage amplitude (V_1 , V_2) and phase (ϕ) are measured over a wide

range of frequencies (0.005 to 10 kHz) of applied current. A reference resistor is used in the process of measurement. The magnitude of the real part of resistivity is determined by the following expression:

$$\rho_{real} = R_{ref} \frac{V_2 - V_1}{V_1} * \frac{S}{L}, \tag{2.8}$$

where R_{ref} is reference resistor resistivity; S is cross section area of the measured sample, and L is the length of the measured sample.

In conclusion, there are three major methods of measurement of IP effect. Chargeability is for the time-domain measurements as the Percentage Frequency Effect (PFE) being the measured parameter in the frequency domain measurements. Complex Resistivity (CR) method measures the magnitude of the complex resistivity and the phase of polarization voltage over a wide range of frequencies.

2.3 GEMTIP Modeling

One of the most important problems of electromagnetic geophysics is to study the frequency-dependent complex resistivity of rocks, in which the IP phenomenon is manifested. Over the past decades, several different conductivity relaxation models have been developed to study the complex resistivity (CR) of rocks, including the empirical Cole-Cole model (Cole and Cole, 1941; Pelton et al., 1978). This widely accepted empirical model describes the frequency dependence of CR reasonably well. However, it does not provide a direct relationship between the CR spectra and rock properties. The generalized effective-medium theory of induced polarization (GEMTIP) was introduced recently in order to provide a link between the petrophysical properties of rocks and their CR spectra (Zhdanov, 2008). GEMTIP is a new and rigorously formulated CR model,

which uses effective-medium theory to describe the resistivity of the multiphase heterogeneous rocks and its relationship with the rocks' physical and electrical properties. Using the GEMTIP theory, we can build the multiphase composite model for the general heterogeneous rocks. The panel (a) of Figure 2.6 shows an effective-medium model of a mineral containing rock with mineral properties including grain size, grain shape, grain eccentricity, volume fraction (porosity), and grain alignment (anisotropy), while panel (b) shows an effective-medium model of a reservoir rock with formation properties like matrix resistivity, grain resistivity, and grain polarizability (Zhdanov et al., 2009).

In the GEMTIP model, a complex heterogeneous rock formation is described as a composite model formed by a homogeneous host medium of a volume *V* with a complex conductivity tensor $\hat{\sigma}_0(\mathbf{r})$ (where $\mathbf{r}$ is an observation point) filled in with grains of arbitrary shape and conductivity. Generally, the rock is composed of a set of *N* different types of grains whose complex tensor conductivity is marked as $\hat{\sigma}_l$ (l = 1, 2, ..., N). The grains of the l^{th} type have a volume fraction f_l in the medium and a particular shape and orientation. To find the effective conductivity tensor ($\hat{\sigma}_e$), we consider the given inhomogeneous composite model as a combination of a homogeneous background whole space with the conductivity tensor $\hat{\sigma}_b$ and the anomalous domains with the anomalous conductivity $\Delta\hat{\sigma}(\mathbf{r})$:

$$\hat{\sigma}(\mathbf{r}) = \hat{\sigma}_b + \Delta\hat{\sigma}(\mathbf{r}). \tag{2.9}$$

According to Zhdanov (2008), we can use the following expression for the effective conductivity of the polarized inhomogeneous medium:

$$\hat{\sigma}_e = \hat{\sigma}_b + \left[\hat{\mathbf{I}} + \hat{\mathbf{p}}_0\right]^{-1}\left[\hat{\mathbf{I}} - \Delta\hat{\sigma}_0^p\hat{\boldsymbol{\Gamma}}_0\right]^{-1} \cdot \left[\hat{\mathbf{I}} + \hat{\mathbf{p}}_0\right] \cdot \Delta\hat{\sigma}_0 f_0 +$$

$$+ \sum_{l=1}^{N}\left[\hat{\mathbf{I}} + \hat{\mathbf{p}}_l\right]^{-1}\left[\hat{\mathbf{I}} - \Delta\hat{\sigma}_l^p\hat{\boldsymbol{\Gamma}}_l\right]^{-1} \cdot \left[\hat{\mathbf{I}} + \hat{\mathbf{p}}_l\right] \cdot \Delta\hat{\sigma}_l f_l, \tag{2.10}$$

where $\hat{\sigma}_e$ is an effective-medium conductivity tensor; $\Delta\hat{\sigma}_l$ is an anomalous conductivity tensor; $\Delta\hat{\sigma}_l^p = [[\hat{\mathbf{I}} + \hat{\mathbf{p}}_l] \cdot \Delta\hat{\sigma}_l$ is the polarized anomalous conductivity; $\hat{\mathbf{p}}_l$ is a surface polarizability tensor; and $\hat{\mathbf{\Gamma}}_l$ is a volume depolarization tensor (l = 1, 2, ..., N). In particular, we consider the background conductivity to be equal to the conductivity of the host medium:

$$\hat{\sigma}_b = \hat{\sigma}_0, \tag{2.11}$$

so that $\Delta\hat{\sigma}_0 = 0$. Then we arrive at the following expression:

$$\hat{\sigma}_e = \hat{\sigma}_0 + \sum_{l=1}^{N} \left[\hat{\mathbf{I}} + \hat{p}_l\right]^{-1} \left[\hat{\mathbf{I}} - \Delta\hat{\sigma}_l^p \cdot \hat{\mathbf{\Gamma}}_l\right]^{-1} \cdot \left[\hat{\mathbf{I}} + \hat{p}_l\right] \cdot \Delta\hat{\sigma}_l f_l. \tag{2.12}$$

This formula provides a mathematical expression of the effective conductivity of an arbitrary multiphase composite polarized medium. Using this formula, we can find the effective conductivity of rocks having inclusions with arbitrary shape and electrical properties.

Let us consider first the case of an isotropic multiphase composite model where all conductivities become scalar functions. In this case, the composite model is formed by a homogeneous host medium of volume V with conductivity (σ_0), which is filled with grains of spherical shape. We assume that there are N different types of grains whose grain radius, conductivity, and surface polarizability are a_l, σ_l, and k_l, respectively. Then the volume depolarization tensors are constant scalar tensors, which are equal to (Zhdanov, 2008):

$$\hat{\mathbf{\Gamma}}_l = \mathbf{\Gamma}_l \hat{\mathbf{I}} = -\frac{1}{3\sigma_b} \hat{\mathbf{I}}. \tag{2.13}$$

According to the definition of the surface polarizability tensor, we have:

$$\hat{p}_l = p_l \hat{\mathbf{I}} = 2\alpha_l {a_l}^{-1} \sigma_b (\Delta\sigma_l)^{-1} \hat{\mathbf{I}}. \tag{2.14}$$

In formula (2.14), α_l is the surface polarizability factor for the l^{th} grain, which is equal to:

$$\alpha_l = \frac{a_l}{2}(2\rho_l + \rho_0)(\tau_l)^{-C_l}, \tag{2.15}$$

where τ_l is the time constant for each grain that determines the length of time required for the decay of the CR curve to a specified level; C_l is the relaxation parameter which controls the rate of decay of the CR curve; and $\rho_l = \sigma_l^{-1}$ is the grain resistivity.

Substituting expression (2.13), (2.14), and (2.15) into expression (2.12) and after some algebra, we arrive at the following GEMTIP expression of the effective resistivity ρ_e for the multiphase composite medium with spherical grains:

$$\rho_e = \rho_0 \left\{ 1 + \sum_{l=1}^{N} \left\{ f_l m_l \left[1 - \frac{1}{1 + (-i\omega\tau_l)^{C_l}} \right] \right\} \right\}^{-1}, \tag{2.16}$$

where:

$$m_l = 3\frac{\rho_0 - \rho_l}{\rho_0 + 2\rho_l},$$

$$\tau_l = \left[\frac{a_l}{2\alpha_l}(\rho_0 + 2\rho_l) \right]^{\frac{1}{C_l}}, \tag{2.17}$$

and ρ_0 is the matrix resistivity of the rock; ρ_l is the resistivity of the l^{th} grain; f_l is the volume fraction of the l^{th} grain; and m_l is chargeability of the l^{th} grain.

Following Zhdanov et al. (2009), we consider now the case of a multiphase heterogeneous medium filled with completely randomly oriented ellipsoidal inclusions. By analogy, we define the empirical surface polarization coefficient α_l as:

$$\alpha_l = \frac{\overline{a_l}}{2}(2\rho_l + \rho_0)(\tau_l)^{-C_l}, \tag{2.18}$$

where $\overline{a_l}$ is an average value of the equatorial (a_{lx} and a_{ly}) and polar (a_{lz}) radius of the

ellipsoidal grains:

$$\overline{a_l} = \frac{a_{lx} + a_{ly} + a_{lz}}{3}, \tag{2.19}$$

As a result, we obtain the following expression for the effective resistivity (Zhdanov et al., 2009):

$$\rho_e = \rho_0 \left\{ 1 + \sum_{l=1}^{N} \frac{f_l m_l}{3} \sum_{a=x,y,z} \frac{2\rho_l + \rho_0}{3h_a} \left[1 - \frac{1}{1 + (-i\omega\tau_l)^{c_l} \dfrac{2h_a}{\lambda_{la}\overline{a_l}(2\rho_l + \rho_0)}} \right] \right\}^{-1}, \tag{2.20}$$

where

$$h_a = \rho_l + \gamma_{la}(\rho_0 - \rho_l). \tag{2.21}$$

Generally, we can consider that the grain resistivity is much smaller than the matrix resistivity: $\rho_l \ll \rho_0$. To simplify the calculations, we introduce new notations:

$$\frac{2h_a}{\lambda_{la}(2\rho_l + \rho_0)} = \frac{2[\rho_l + \gamma_{la}(\rho_0 - \rho_l)]}{\lambda_{la}(2\rho_l + \rho_0)} \approx \frac{2\gamma_{la}}{\lambda_{la}} = r_a, \tag{2.22}$$

$$\frac{2\rho_l + \rho_0}{3h_a} = \frac{2\rho_l + \rho_0}{3[\rho_l + \gamma_{la}(\rho_0 - \rho_l)]} \approx \frac{1}{3\gamma_{la}}, \tag{2.23}$$

$$m_l = 3\frac{\rho_0 - \rho_l}{\rho_0 + 2\rho_l} \approx 3. \tag{2.24}$$

Using these notations, we arrive at the following expression for the effective resistivity:

$$\rho_e = \rho_0 \left\{ 1 + \sum_{l=1}^{N} f_l \sum_{\alpha=x,y,z} \frac{1}{3\gamma_{l\alpha}} \left[1 - \frac{1}{1 + (-i\omega\tau_l)^{c_l} \dfrac{r_\alpha}{\overline{a_l}}} \right] \right\}^{-1}. \tag{2.25}$$

Generally, we consider the equatorial radii of the ellipsoidal grains to be the same ($a_{lx} = a_{ly}$), so the ellipticity of the rotational ellipsoid is equal to $e = \frac{a_{lz}}{a_{lx}} = \frac{a_{lz}}{a_{ly}}$. The

coefficients γ_{la} and λ_{la} are the structural parameters defined by geometrical characteristics of the ellipsoidal inclusions, and they are functions of ellipticity *e*:

$$\gamma_{la} = \frac{3V}{8\pi}\int_0^\infty \frac{ds}{(s+a_{lj})R_S}, j = x, y, z, \tag{2.26}$$

where

$$R_S = \sqrt{\prod_{j=x,y,z}(s+a_{lj})}\,,$$

$$V = \frac{4\pi a_{lx}a_{ly}a_{lz}}{3}. \tag{2.27}$$

Using the notations, $a_{lx} = a_{ly} = a$ and $a_{lz} = b$, we obtain the following expression for the surface depolarization tensor:

$$\widehat{\Lambda} = -\frac{1}{\sigma_b}\begin{bmatrix}\lambda & 0 & 0\\ 0 & \lambda & 0\\ 0 & 0 & \lambda_z\end{bmatrix}, \tag{2.28}$$

where

$$\lambda = \frac{ab^3}{2}\int_0^b \frac{[2a^2b^2-(b^2-a^2)z^2](b^2-z^2)}{[a^2b^2+(b^2-a^2)z^2]^{5/2}\sqrt{b^4-(b^2-a^2)z^2}}dz, \tag{2.29}$$

$$\lambda_z = ba^3\int_0^b \frac{[3b^4-a^2b^2-(b^2-a^2)z^2]z^2}{[a^2b^2+(b^2-a^2)z^2]^{5/2}\sqrt{b^4-(b^2-a^2)z^2}}dz. \tag{2.30}$$

Table 2.1 shows a descriptive guide for all the GEMTIP parameters mentioned above.

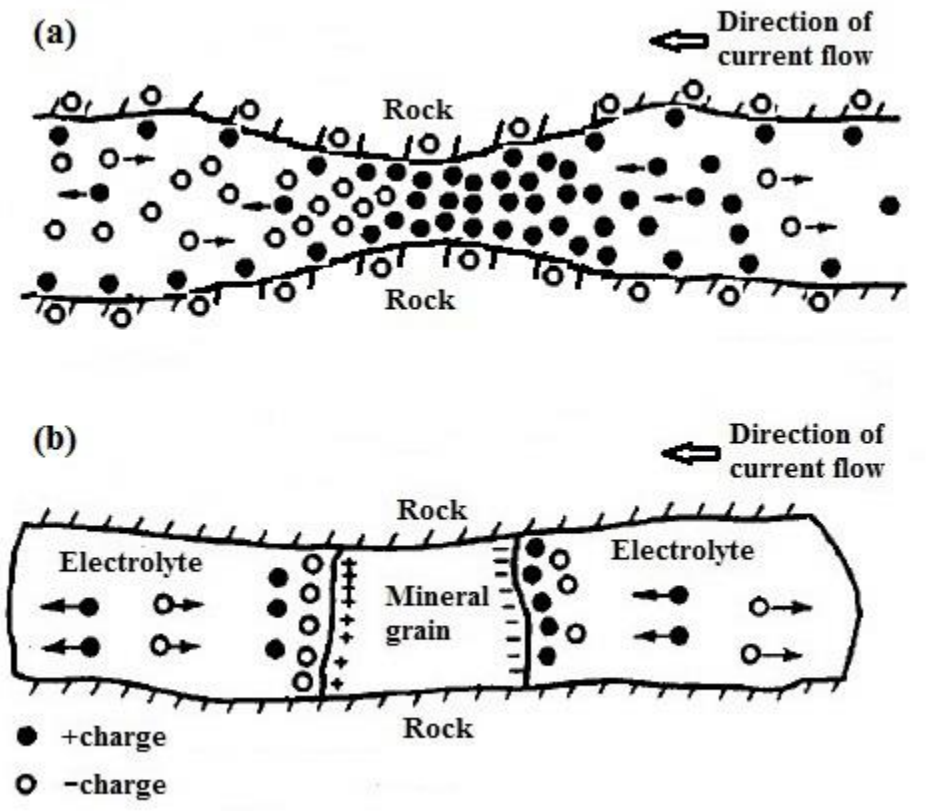

Figure 2.1. Membrane and electrode polarization effects (adapted from Cambridge University Press, 1990). (a) Membrane polarization in a porous sandstone due to the a narrow pore channel; (b) Electrode polarization.

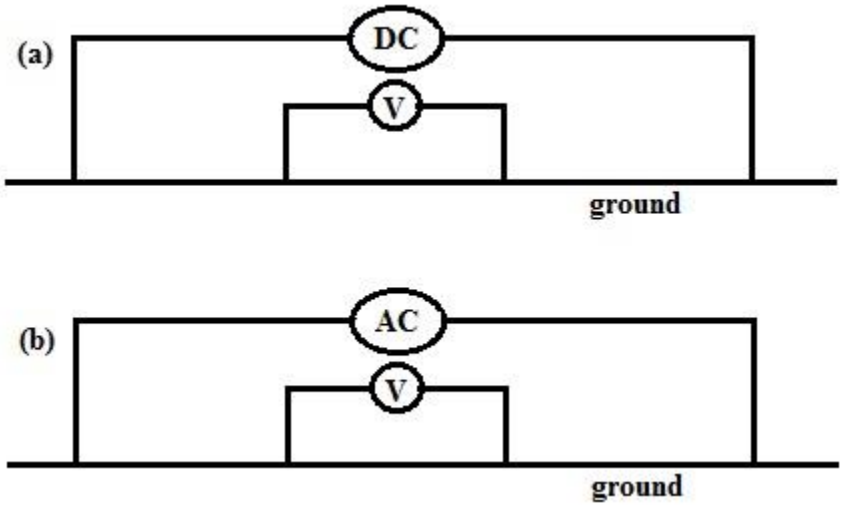

Figure 2.2. Example of measuring IP effect using the Wenner array. (a) Time-domain method. (b) Frequency-domain method.

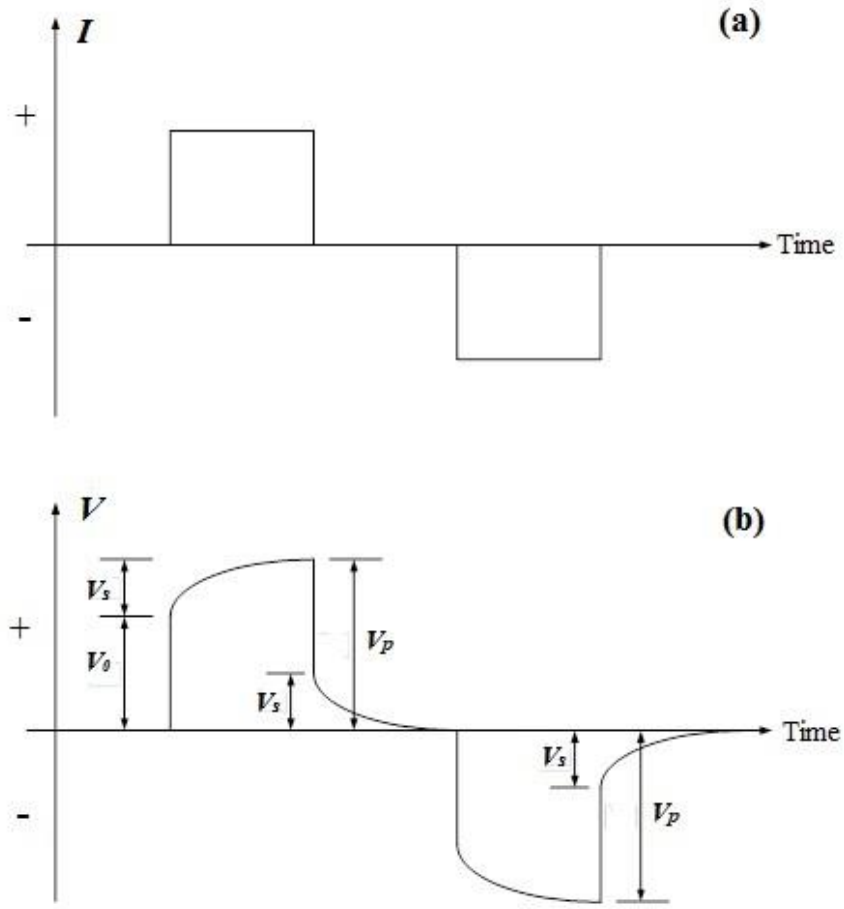

Figure 2.3. Representation of IP effect in time domain. (a) Transmitted current waveform vs. time. (b) Recorded voltage waveform vs. time.

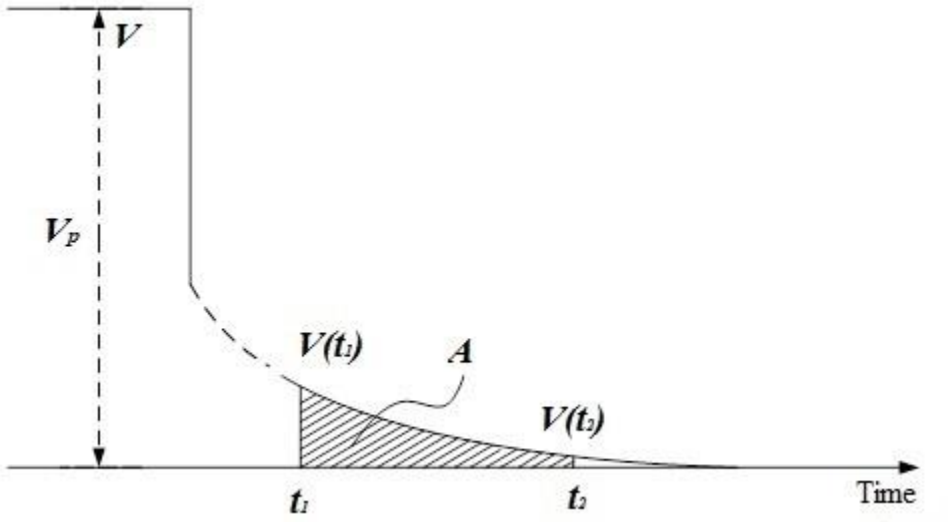

Figure 2.4. The integrated decay voltage curve used as a measurement of chargeability.

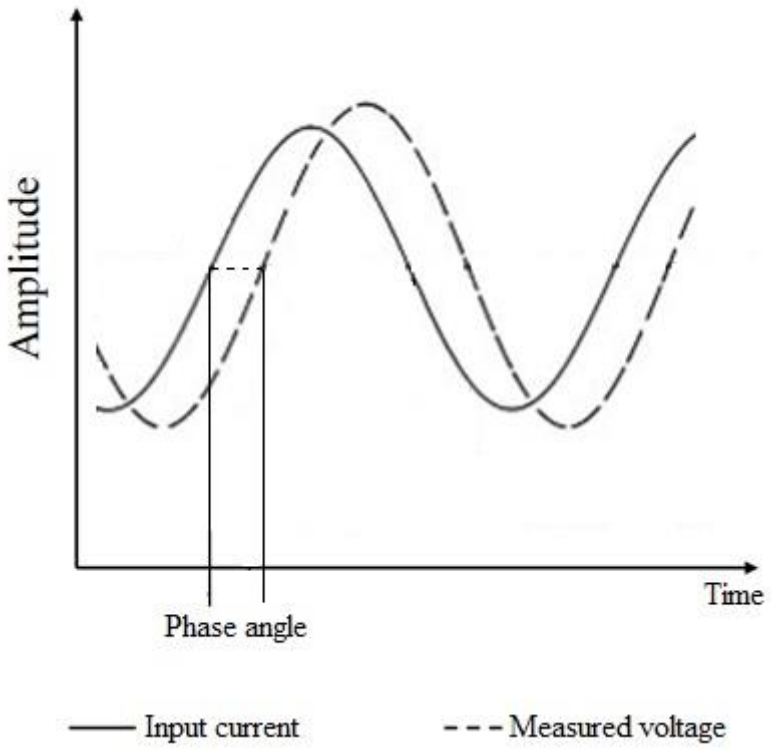

Figure 2.5. Frequency-domain IP measurements. The waveform of an applied alternating current and the waveform of the corresponding measured voltage at the receiver are observed and the phase angle is measured.

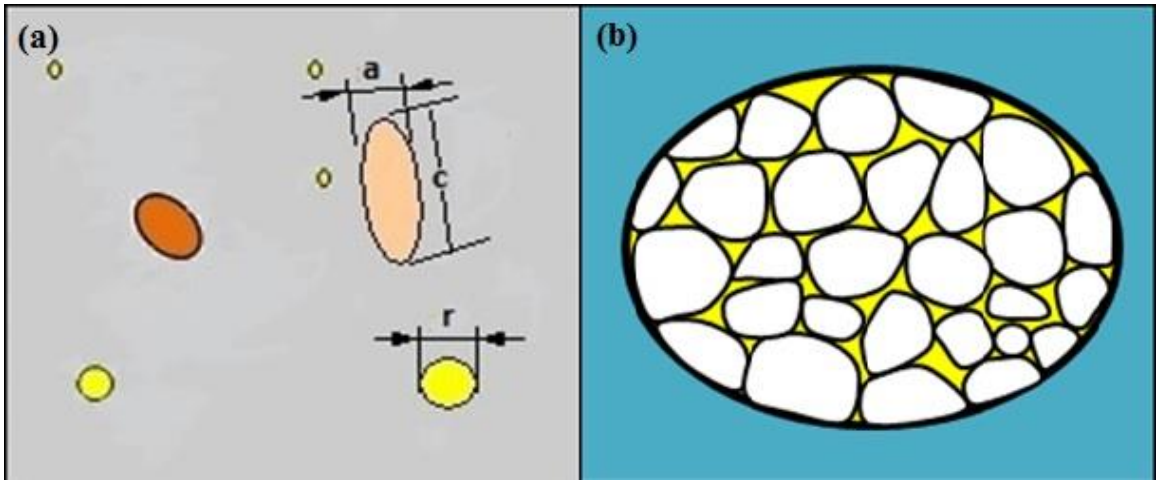

Figure 2.6. Multiphase composite model of general heterogeneous rocks. (a) An effective-medium model of a mineral containing rock; (b) an effective-medium model of a reservoir rock.

Table 2.1. Descriptive guide for GEMTIP parameters.

Parameter	Units	Name	Description
$\widehat{\boldsymbol{\sigma}}_{\mathbf{0}}$	-	conductivity tensor	conductivity tensor of host medium
$\widehat{\boldsymbol{p}}_{\boldsymbol{l}}$	-	surface polarizability tensor	tensor of polarizability on the surface between the l^{th} grain and the surrounding fluid
$\widehat{\boldsymbol{\Gamma}}_{\boldsymbol{l}}$	-	volume depolarization tensor	tensor of depolarization through the entire body of the l^{th} grain
$\boldsymbol{\Delta\widehat{\sigma}_l}$	-	anomalous conductivity tensor	anomalous conductivity tensor of the l^{th} grain
$\boldsymbol{\rho_e}$	$\Omega.m$	effective resistivity	resulting effective resistivity
$\boldsymbol{\rho_0}$	$\Omega.m$	matrix resistivity	matrix resistivity of rock
$\boldsymbol{\rho_l}$	$\Omega.m$	grain resistivity	resistivity of the l^{th} grain
$\boldsymbol{f_l}$	%	grain volume fraction	volume fraction of the l^{th} grain
$\boldsymbol{m_l}$	-	grain chargeability	chargeability of the l^{th} grain
$\boldsymbol{\tau_l}$	s	time constant	time constant of the l^{th} grain
$\boldsymbol{C_l}$	-	relaxation parameters	relaxation coefficient
$\boldsymbol{\omega}$	Hz	angular frequency	EM angular frequency
$\boldsymbol{a_l}$	m	grain radius	radius of the l^{th} grain
$\boldsymbol{\alpha_l}$	m	surface polarizability	charge behavior on the l^{th} grain
$\boldsymbol{e_l}$	-	ellipticity	ratio between a_{lz} and a_{lx}

CHAPTER 3

METHODS OF GEMTIP MODEL INVERSION USING GENETIC ALGORITHMS

3.1 Studying the Effects of GEMTIP Parameters on CR Curve

The forward modeling of the GEMTIP resistivity model is the key to understanding the relationship between the GEMTIP parameters and the complex resistivity. Generally, two analytical GEMTIP models can be used for modeling rock resistivity, which are spherical model and the ellipsoidal model, respectively. A previous research (Phillips, 2010) studied the spherical GEMTIP model. In this section, the two-phase ellipsoidal GEMTIP model was tested by varying its parameters – DC resistivity (ρ_0), ellipticity (e), time constant (τ), relaxation parameter (C), and the volume fraction (f). In the case of a two-phase ellipsoidal GEMTIP model, the effective resistivity can be calculated as follows:

$$\rho_e = \rho_0 \left\{ 1 + f \sum_{\alpha=x,y,z} \frac{1}{3\gamma_\alpha} \left[1 - \frac{1}{1 + (-i\omega\tau)^C \frac{2\gamma_{la}}{\lambda_{la}\bar{a}}} \right] \right\}^{-1}, \qquad (3.1)$$

where the coefficients γ_{la} and λ_{la} are functions of ellipticity e, and $\bar{a}$ is the average value of the equatorial (a_x and a_y) and polar (a_z) radius of the ellipsoidal grains.

In what follows, several synthetic models were created to reveal how GEMTIP

parameters affect the real and imaginary resistivity curves. Tables 3.1 - 3.5 show the parameter settings of the two-phase ellipsoidal GEMTIP.

Figure 3.1 shows real and imaginary resistivity curves obtained by varying ellipticity (e). In this case, five different values of e are chosen from the reasonable range, which are 0.1, 0.5, 1, 5, and 10, respectively. It is very clearly shown that the resistivity curve is very sensitive to the ellipticity. Ellipticity e = 1 represents the two-phase spherical GEMTIP model. Ellipticity e = 0.1 and e = 0.5 represent the oblate spheroid, while e = 5 and e = 10 represent the prolate spheroid. By comparing these curves, we can see that both the real and imaginary resistivities decrease when the ellipticity increases in the range of $[0, 1]$; on the contrary, the resistivities increase if the ellipticity increases in the range of $[1, 10]$.

The main purpose of this thesis is to study the ellipsoidal GEMTIP model, so in the following forward models the value of elliipticity is set as 10. Figure 3.2 shows real and imaginary resistivity curves obtained by varying volume fraction (f). From the modeling result, we can see that both real and imaginary resistivity curves are shifted with the increase of volume fraction.

Figure 3.3 shows real and imaginary resistivity curves obtained by varying relaxation parameter (C). The relaxation parameter appears to affect the amplitude of both real and imaginary resistivities. The typical range of C is $[0, 1]$. A previous IP study (Pelton, 1978) suggested that the relaxation parameter should not be equal to 1. However, large values of C tend to cause a dramatic decrease of real resistivity in the lower frequency areas, and a sharp resistivity peak in the imaginary part.

Figure 3.4 shows the real and imaginary resistivity curves obtained by varying time constant (τ). The variations of time constant change the amplitude of the real part.

Emond (2007) pointed out that decreasing the grain size was analogous to decreasing the time parameter, which causes the peak of imaginary resistivity moving into the higher frequency range.

Figure 3.5 uses five synthetic models to show how DC resistivity (ρ_0) affects the CR curve. It is obvious that the effective resistivity increases with the DC resistivity.

To summarize the randomly oriented ellipsoidal GEMTIP model, time constant (τ) affects the location of the peak of CR curve, DC resistivity (ρ_0), and relaxation parameter (C) may affect the amplitude of the curve, and fraction volume (f) and ellipticity (e) can affect both. It is obvious that the imaginary part of the resistivity is much more sensitive to the changes of the GEMTIP parameters than the real part. Among all the parameters, the CR curve is the most sensitive to the matrix resistivity (ρ_0) because a small change of ρ_0 results in large changes of effective resistivity, and fewer sensitivities to the time constant (τ), relaxation parameter (C), ellipticity (e), and fraction volume (f). Thus, in the following chapter, the fraction volume (f) is obtained independently.

3.2 Inversion of GEMTIP Model Parameters

The purpose of this inversion is to recover all the GEMTIP parameters from the measured IP data. We consider the GEMTIP inverse problem for a three-phase ellipsoidal GEMTIP model, which depends on the nine GEMTIP parameters - ρ_0, f_1, C_1, τ_1, e_1, f_2, C_2, τ_2 and e_2, introduced in the previous section. We denote by **m** the vector of the unknown model parameters:

$$\mathbf{m} = [\rho_0,\ f_1,\ C_1,\ \tau_1,\ e_1, f_2,\ C_2,\ \tau_2,\ e_2]. \tag{3.2}$$

The values of the CR resistivity at different frequencies, $\rho_{ei} = \rho_e(\omega_i)$, from the vector **d** of the observed data:

$$\mathbf{d} = [\rho_{e1},\ \rho_{e2},\ \ \ldots,\ \rho_{en}]. \tag{3.3}$$

Fundamental GEMTIP equation (2.17) can be used to obtain the nonlinear relationships between CR data and the GEMTIP parameters, which in compact form can be written as the following operator equation:

$$\mathbf{d} = \mathbf{G}_{\boldsymbol{IP}}(\mathbf{m}). \tag{3.4}$$

The GEMTIP inversion is based on minimization of the following misfit functional:

$$\phi(\mathbf{m}) = \|\mathbf{d} - \mathbf{G}_{\boldsymbol{IP}}(\mathbf{m})\|^{\mathbf{2}} = \min, \tag{3.5}$$

where we use a standard least-square norm.

One can use different minimization methods for solving equation (3.5). For example, the regularized conjugate-gradient (RCG) method was used by Fu (2013). However, in some situation, e.g., in the case of three-phase ellipsoidal GEMTIP model with nine unknown GEMTIP parameters, the RCG algorithm experiences difficulty in converging into the global minimum. Figure 3.6 shows a contour map of the misfit functional calculated for a three-phase ellipsoidal GEMTIP model as a function of two parameters, ρ_0 and f_1. The noise rate of the calculated CR is 5%. The pentagon shows the position of the true values of these two parameters. From this figure, we can see a narrow dark-blue low-misfit area, which may easily lead the RCG inversion falling into the local minima. If all nine GEMTIP parameters vary, the number of the local minima may significantly increase. Besides, it is very time-consuming to calculate the Fréchet derivative for the GEMTIP forward modeling operator, $\mathbf{G}_{\boldsymbol{IP}}$. It is possible to use the global minimum search (GMS) method to find the globally optimal solution (e.g., Fu, 2013). This method defines the sample interval in the search spaces for each GEMTIP parameter and calculates the misfit for every possible solution from the sampling space to

produce the one which has the smallest value. However, this method is very time-consuming and inefficient. I consider an alternative approach based on hybrid adaptive genetic algorithm with simulated annealing (SAAGA) for the GEMTIP inversion, which will be discussed in details in the following sections.

3.3 Pure Genetic Algorithm

In recent years, intelligent global minimum search algorithms have become widely used for the nonlinear inversions. Similar to the Monte Carlo method (e.g., Hammersley and Handscomb, 1964), these algorithms are based on repeated random sampling and different kinds of physical or biological rules to evolve the best solution. For example, the genetic algorithm (GA) (Holland, 1975; Goldberg, 1989) is a heuristic search method that mimics the process of natural evolution. Simulated annealing (SA) algorithm (Kirkpatrick et al., 1983) comes from annealing in metallurgy, a technique involving heating and controlled cooling of a material.

A lot of geophysical inverse problems are nonlinear and tend to have multimodal objective functions (Sen and Stoffa, 1992). Sometimes the inversion results cannot reach the global minimum using the conventional gradient-type inversion methods such as regularized conjugate-gradient (RGC) method, so it is necessary to apply a more sophisticated approach. A genetic algorithm (GA) is a good example of this approach. Generally, GA is an effective optimization method for many geophysical inverse problems where some traditional methods fail (Parker, 1999; Lin, 2012). It has the following advantages:

1. Optimization with continuous or discrete parameters, and with small sample intervals;
2. No need to calculate derivatives;

3. Solving multidimensional and nondifferential problems;
4. Solving minimization problems with multiple local minima.

These advantages of a GA method make it very suitable for the GEMTIP inverse problem. In this thesis, we apply first a pure genetic algorithm for the GEMTIP model inversion. In a pure genetic algorithm, a population of candidate solutions (individuals) for an optimization problem is evolved toward better solutions. Traditionally, the solutions are coded in binary form as strings of 0s and 1s to be mutated and altered. Figure 3.7 shows the flow chart of the GA method. The evolution starts from a population of randomly generated solutions from the search space and proceeds as an iterative process. The population in each iteration is called a generation. In each generation, the fitness of every individual is evaluated by an objective functional (e.g., the reciprocal of misfit given by equation (2.25)). The individuals who have high fitness are stochastically selected from the current population, and then they are chosen to form a new generation by applying genetic operations (mutation and crossover). The above steps run iteratively until the inversion process meets the termination condition. The detailed steps of the pure GA are as follows:

1. Objective Functional:

$$\phi = \|\mathbf{G}_{\boldsymbol{IP}}(\mathbf{m}) - \mathbf{d}\|/\sqrt{N} \tag{3.6}$$

   where N is the number of observed CR data.

2. Search space and search interval: Before the inversion, the search space is defined for each GEMTIP parameters. The search space of matrix resistivity (ρ_0) depends on the observed values of the effective resistivities. Theoretically, the suggested ranges for e, τ, and C are $[1, 10]$, $[0, 10]$, and $[0, 1]$, respectively. The extreme values of f are 0% and 100%, so the search space of this parameter is $[0, 100]$ in the unit of percent.

Generally in a GA method, the search space is divided into 2^n segments (n=1, 2, …, 20), where the number n depends on the conventional memory of the computer. In this thesis, the number of segments is set on 2^{10} based on several numerical tests. Table 3.6 shows an example of the definition of search space and search interval for a synthetic CR data test.

From this table, each search space is divided into 1024 segments, so the search interval is small enough to guarantee the accuracy of the GA method.

3. Initial population and individual: A possible solution is randomly generated from the search spaces of each GEMTIP parameter, which is called an individual. Then I use binary to code each parameter into a string, and connect these strings one by one to form an individual which presents an encoded parameter model. Table 3.7 shows an example of the formation of an individual. Finally, I repeat the above steps Q times and obtain Q individuals to form the initial population (or generation). The population size is one of the factors that influence the computing time and the inversion result. It should be large enough to guarantee the diversity of the initial population so that the population might contain some solutions with low misfits. On the contrary, larger population size will result in increasing the computing time to evaluate each individual and decreasing the chance to select better individual. Based on several numerical tests, the size of population Q is set to be 150.
4. Fitness functional. The fitness value is the most important parameter to measure each individual from the population. For a better solution, the fitness should be larger so that it might have higher chance to be selected in the following step. In this inversion, there are three ways to define the fitness function:

$$\text{(i) } f(i) = \phi(i)^{-1} \qquad i = 1, 2, \dots, Q$$

$$\text{(ii) } f(i) = \phi_{max} - \phi(i) \quad i = 1, 2, \dots, Q$$

$$\text{(iii) } f(i) = 1/\sum_{j=1}^{Q} e^{\frac{\phi(i)-\phi(j)}{2\sigma}} \quad i = 1, 2, \dots, Q \tag{3.7}$$

where f is the fitness function; ϕ is the misfit function; and σ is the standard deviation of $\phi(i)$. One can simply use the reciprocal of the misfit function (i) or the linear differential function (ii) to calculate the fitness based on the misfit value. However, of all the three definitions above, the third one (iii) is recommended because using this function the fitness values of all the individuals will follow the probability distribution. Thus, for a possible solution of the three-phase ellipsoidal GEMTIP model which has a small misfit value, the fitness value of the third function is larger than those of the other two functions, so that the chance of selection can be increased.

5. Selection: The "roulette rule" is used to determine which individual should be selected. The chances are higher for the good individuals which have larger fitness values.

   Firstly, the fitness function is transformed as follows:

$$f(i) = f(i)/\sum_{i=1}^{Q} f(i). \tag{3.8}$$

   Secondly, the "roulette" space for each individual is defined as follows:

$$\mathrm{S}(i) = \sum_{j=1}^{i} f(j). \tag{3.9}$$

   Thirdly, a randomly generated number a ($0 \le a \le 1$) is used to determine the reproduction chance of each individual. If $\mathrm{S}(i-1) \le a \le \mathrm{S}(i)$, then the i^{th} individual will be selected. This step is repeated for Q times to form a new generation with the

same population size.

6. Crossover and mutation: It has been well established in a lot of GA publications that moderately large values of crossover probability P_e (0.5< P_e <1.0), and small values of mutations probability P_m (0.001< P_m <0.05) are essential for the successful working of GAs. The moderately large values of P_e promote the extensive recombination of schemata, while small values of P_m are necessary to prevent the disruption of the solutions. Based on several numerical tests, the parameters setting that P_e=0.65 and P_m=0.003 is suitable for the synthetic CR data inversion.
   - Crossover: For each two selected individuals, a crossover point is randomly selected to cut these parent chromosomes into two parts. If a randomly generated number a ($0 \leq a \leq 1$) is larger than the crossover probability (P_e), then exchange the chromosome parts to form a pair of offspring. Figure 3.8 (a) shows an example of the crossover operation.
   - Mutation: For each number of the offspring which are generated from the previous step, it has a very small chance to switch the number 0 into 1 or 1 into 0 if a randomly generated number a ($0 \leq a \leq 1$) is smaller than the mutation probability (P_m). Figure 3.8 (b) shows an example of the mutation operation.
7. Termination condition: In this thesis, three termination conditions are set for the numerical test:

   (i) If the misfit of the imaginary part is lower than a certain level (e.g., 3%), or

   (ii) If the number of generations reaches a certain number (e.g., 30000), or

   (iii) If all the selected individuals are the same.

   If the inversion result satisfies the second termination condition, then it means the misfit cannot meet the first condition, so the solution with the lowest misfit from

the generations is chosen to be the final inversion result.

All the numerical tests have been implemented using a code written in FORTRAN.

To test the pure genetic algorithm, I have used the synthetic CR data, which are obtained from the forward modeling considering a model formed by a homogeneous host rock filled with two types of grains with two grain sizes. This synthetic model comprises a rock matrix with the resistivity 200 $\Omega.m$ and two inclusions with grain ellipticities of 4.0, and 1.0, respectively. The known values of the time constant, relaxation parameter, and volume fraction of these two inclusions are 0.9, 0.9, 10%, and 0.01, 0.9, 15%, respectively. All the parameters are summarized in the Table 3.8. The termination condition is set that the misfit of imaginary CR is less than 1%. Figure 3.9 represents both the synthetic and predicted resistivity curves for three-phase ellipsoidal GEMTIP model plotted against frequency. It clearly shows that there are two maximum IP responses in the imaginary part for the three-phase ellipsoidal GEMTIP model. The synthetic curve came from using the true model parameter value, while the predicted data were obtained by the pure genetic algorithm. The predicted data fit the synthetic data very well. In this inversion, after 28937 iterations (time cost is about 2200s) the correct model parameters were recovered. The final misfit is 0.5%, where Figure 3.10 shows the misfit plot.

This result demonstrates that the pure GA method can be used for the inversion of GEMTIP data. Compared to the global minimum search (GMS) method (e.g., Fu, 2013), GA takes just 30 minutes of computations to get the global minimum, which is much smaller than the inversion time of the GMS method (~5 h). However, there are two main weaknesses of using GA:

1. GA is very sensitive to the probabilities of crossover and mutation. A very small

change in these probabilities may lead the inversion result into the local minimum.

2. In most cases, GA has a tendency to converge towards local minima rather than to the global minimum of the inverse problem. Once GA jumps into a local minimum area, sometimes it is very difficult for this method to get out of this area. Table 3.9 shows an example from the previous numerical test. In that inversion result, the probabilities of crossover (P_e) and mutation (P_m) were set as 0.65 and 0.003, respectively. Under this setting of the GA's parameters, after 33 iterations the recovered matrix resistivity ρ_0 converges into the true value, 200. If I change the mutation probability (P_m), for example, to 0.004 or 0.002, then the inversion result converges into some local minima. Figure 3.11 shows positions of ρ_0 and f_1 for the three cases within the misfit contour map. The red pentagon indicates that the recovered parameters are consistent with the synthetic model when P_m equals to 0.003. However, the green ($P_m = 0.004$) and pink ($P_m = 0.002$) pentagons show the inversion results do not converge to the global minimum area. One possible solution is to increase the mutation probability, but that will transform the GA into a pure random search method. For example, in the previous inversion result shown, GA took about thirty thousand iterations to meet the termination condition.

In short, the pure GA method has its own problems. Varying the amount of mutation presents a trade-off problem between diversity and performance. Maintaining diversity is a prominent consideration. Genetic algorithm using selection alone cannot generate solutions outside the population. Crossover and mutation generate new solutions, but with certain limitations. Crossing nearly identical strings yields offspring similar to the parent strings, so crossover cannot reintroduce diversity. Mutation can generate the full solution space, but may take an excessively long time to yield a desirable solution, or

even transforms the pure GA method into a simple random search method. In addition, it is not easy to regulate the GA's convergence. A generally effective method for setting parameters (population size, mutation probability, and crossover probability) has not yet been developed, because the optimal parameters are problem-dependent. To make the improvements, in the next section, I apply the adaptive genetic algorithm (AGA) and the hybrid genetic algorithm with simulated annealing (SAGA) to the GEMTIP inversion method.

3.4 Hybrid Adaptive Genetic Algorithm with Simulated Annealing (SAAGA)

3.4.1 Adaptive Genetic Algorithm

In a pure GA method, the probabilities of crossover and mutation are constant. High probabilities are necessary in the first several generations to insure the population diversity. However, after hundreds of generations, it is not good to apply fixed probabilities to all individuals. For individuals that have larger fitness, we want their probabilities of changes will be smaller than others. So it is better to apply adaptive probabilities of crossover and mutation. In this thesis, the adaptive genetic algorithm is applied to adjust probabilities of crossover and mutation in each generation (Srinivas, 2002) according to the following formula:

$$P_e = \begin{cases} P_e \dfrac{f_{max} - f'}{f_{max} - f_{avg}}, f' \geq f_{avg} \\ P_e, f' < f_{avg} \end{cases}, \tag{3.10}$$

$$P_m = \begin{cases} P_m \dfrac{f_{max} - f}{f_{max} - f_{avg}}, f \geq f_{avg} \\ P_m, f < f_{avg} \end{cases}, \tag{3.11}$$

where P_e is the crossover probability; P_m is the mutation probability; f_{avg} is the mean fitness of all the individuals; f_{max} is the maximum fitness of all the individuals; f' is the fitness of the larger one of two cross individuals; f is the fitness of the individual which will be mutated. In this case, when the fitness is close to the maximum fitness, then the probabilities decrease; otherwise the probabilities do not change.

After applying this method, the misfit plot becomes stable, and the number of iterations that the inversion algorithm requires is much smaller than before. The program usually stops by the third termination condition (All selected individuals are the same). But the inversion result still depends on the setting of GA's parameters (e.g., probabilities of crossover and mutation).

3.4.2 Hybrid Genetic Algorithm with Simulated Annealing

Simulated annealing (SA) is an optimization technique, which was introduced based on the concept of cooling of a material. The name and inspiration come from a technique involving heating and controlled cooling of a material to increase the size of its crystals and reduce their defects. This algorithm starts with a high temperature T_e and an arbitrary initial state. A neighborhood operator is applied to the current state i (having fitness E_i) to yield state j (having fitness E_j). If $E_i < E_j$, then j becomes the current state. Otherwise j becomes the current state with probability, $e^{(E_j - E_i)/T_e}$ (if j is not accepted, i remains the current state). The application of the neighborhood operator and the probabilistic acceptance of the newly generated state are repeated either for a fixed number of iterations or until a quasi-equilibrium is reached. The entire above described procedure is performed repeatedly, each time starting from the current state i and from a lower temperature T_e. What distinguishes the SA algorithms from other globally

optimization method is the criterion by which the newly generated state is accepted or rejected. This criterion should guarantee that the solution will not stay at the local minima areas. Thus, the SA method can guarantee the convergence, but its low speed is the main weakness.

As we discussed, the pure GA was not a good solution for GEMTIP inverse problem. To improve it, we needed to introduce some inversion method to enhance its global search capability. Brown et al. (1989) presented a new method called hybrid genetic algorithm with simulated annealing (SAGA). Figure 3.12 shows the flow chart of the SAGA method. Each iteration of SAGA consists of one or several generations of a GA, followed by a full schedule of SA on each individual. To maintain good solutions produced by the GA method, the SA algorithm begins at a lower temperature.

The detailed processes of the SAGA method consist of the following steps, outlined below, and the Table 3.10 shows all the SA parameters used in the GEMTIP inversion.

1. Obtain all the individuals from the GA method (*X1*).
2. Initialize the following parameters for SA.

a) T_e - initial temperature: For the SA method, a high initial temperature may increase the chance of obtaining the global minimum, but it costs significant computing time. On the contrary, a low initial temperature may influence the global optimum search capability. In the GEMTIP inversion, it is better to use a low initial temperature because we do not need the current models from GA changing too much. The suggested range for T_e is $[5, 500]$. By testing several values from this range, we found that the value of 120 is the best.

b) λ_T - temperature reduction factor: Generally, the range for temperature reduction

factor is $[0.5, 0.99]$. The common value range suggested by Corana et al. (1987) is $[0.85, 0.95]$. In this analysis, we selected 0.85 for this parameter

c) *VM* - step length for the current model: In a SA method, the initial step length does not affect the rate of convergence. In this analysis, I randomly selected five times the search interval as the initial step length for each GEMTIP parameter.

d) *NS* - number of the cycles before the *VM* is adjusted.

e) *NT* - number of iterations before temperature reduction.

These two parameters are called cooling velocity. The optimal parameters are problem dependent. In this analysis, I used an algorithm that puts particular emphasis on the GA method, as the SA algorithm is used for preventing the solutions from falling into local minima areas. If too much emphasis is placed on the SA method, then the genetic characteristics from the GA method will be eliminated. So a high cooling velocity is better for GEMTIP inversion. Based on several numerical tests, I established that *NS*=5 and *NT*=2 are appropriate for the inversion.

3. Generate a new model *X2=X1+VM* to all the individuals which are generated from GA method.

4. Calculate the fitness difference between the current model and the new model:

$$\Delta t = f(X2) - f(X1), \tag{3.12}$$

where f is the fitness functional described previously.

5. If $\Delta t > 0$, then we accept new model *X2*; otherwise we accept the new model if:

$$a < e^{\Delta t / T_e}, \tag{3.13}$$

where *a* is a random number generated from the interval, [0,1].

6. If the program reaches *NS*, then we adjust step length *VM* as follows:

$$\mathrm{VM} = \begin{cases} VM * \left(1 + \dfrac{2 * (R - 0.6)}{0.4}\right), R > 0.6 \\ \dfrac{VM}{1 + \dfrac{2 * (0.4 - R)}{0.4}}, R < 0.4 \\ VM, 0.4 \leq R \leq 0.6 \end{cases}, \tag{3.14}$$

where *R* is the ratio of accepted moves among all the moves. This function guarantees that the ratio of accepted moves is constrained within a fixed range.

7. If the program reaches *NT*, then the temperature T_e decreases:

$$T_e = T_e * \lambda_T. \tag{3.15}$$

By combining the AGA with the SAGA method, I introduce a new method called hybrid adaptive genetic algorithm with simulated annealing (SAAGA). I applied this new method to the inverse problem of the three-phase ellipsoidal GEMTIP model in the case studies described below. In the framework of the SAAGA method, even if the probabilities of crossover and mutation are changed, the result still converges into the global minimum.

To examine the dependence of the crossover probability (P_e) and mutation probability (P_m) for this method, two different probabilities combinations were tested for the synthetic CR data of Table 3.8 in the following two cases, described below. The stopping condition is set as the misfit of the imaginary CR is lower than 0.7%.

- Case (1): $P_e = 0.65$, $P_m = 0.006$.

The program reached the global minimum at the iteration number 1816 (computation time = 3011s). Figures 3.13 and 3.14 show the inversion result and the misfit plot for case (1). Table 3.11 presents the true model parameters and the predicted GEMTIP variables for this case.

- Case (2): $P_e = 0.60$, $P_m = 0.005$.

The program was terminated at iteration number 607 (computation time = 951s). Figures 3.15 and 3.16 demonstrate the inversion results and misfit plot for case (2). Table 3.12 presents the true model and the predicted GEMTIP variables for case (2).

From these inversion results, we can see that the predicted GEMTIP parameters are very close to the true model; and the rate of convergence is faster and more stable than that of the pure GA. The comparison of the misfit plots obtained by these two cases shows even the probabilities of crossover and mutation vary in the certain ranges, the inversion result still converge.

In addition, 3% random noise is added to the synthetic model to examine the SAAGA method. The crossover probability (P_e) and mutation probability (P_m) are set as the same as case (2). The stopping condition is set as the misfit of the imaginary CR is lower than 3%.

- Case (3): $P_e = 0.60$ and $P_m = 0.005$ with 3% random noise

The program reached the global minimum at the iteration number 255 (computation time = 400s). Figures 3.17 and 3.18 show the inversion result and the misfit plot for case (3). Table 3.13 presents the true model parameters and the predicted GEMTIP variables for this case.

Since the stopping condition is more relaxed than those of cases (1) and (2), the program reached the given misfit earlier. Although 3% random noise may increase the difficulty to obtain the global minimum solution, the predicted GEMTIP parameters are still very close to the true values. Again, the predicted curves fit the synthetic curves very well for both real and imaginary resistivities. Thus, the synthetic model study demonstrates that the SAAGA method provides a suitable solution for the inverse problem of the three-phase ellipsoidal GEMTIP model.

3.5 SAAGA with Multipoint Crossover Operation

In the previous section, the hybrid adaptive genetic algorithm with simulated annealing (SAAGA) method is applied to the inverse problem of the three-phase ellipsoidal GEMTIP model and successfully recovered the GEMTIP parameters for the synthetic model. However, for the real rock samples, in some rare circumstances when the observed CR curve of the rock sample is extremely complicated (e.g., flat peak of the CR curve; no peak of the CR curve), this method cannot obtain the global minimum solution. In this chapter, I will propose a modified hybrid genetic algorithm based on the SAAGA method and the multipoint crossover operation for these particular cases. Compared with the global minimum search (GMS) method and the SAAGA method, the case studies indicate that using the SAAGA with multipoint crossover operation the inversion results have been significantly improved.

Generally, a single-point crossover operation is applied for recombination throughout all generations in most of the applications of GAs. The main function of the crossover operation is to transfer good characteristics from the parents to next generation, which determines the solution quality and computational efficiency. Thus, the redesigning of new crossover operations is one of the possible solutions to recover the GEMTIP parameters from the complicated Observed CR data. The use of multipoint crossover operations in GAs has been studied in several researches. Spears (1992) proposed an adaptive crossover operation which varies between two-point and uniform crossover. He concluded that this operation works well especially with larger population size. Then, an advanced adaptive operation, in which either multiple crossover per couple (MCPC) or multiple crossover on multiple parents (MCMP) strategy is used, is developed by Gallard et al. (2000). And Yoon et al. (2002) used several different crossover selection

strategies to study the synergy among multiple crossover operations. They concluded that careful combination of multiple crossover operations can produce synergy, and these combinations are problem-dependent.

In order to develop an effective inversion method for the particular cases when the SAAGA method fails, the three-point crossover operation is applied to the SAAGA method. During the numerical simulations, several multipoint crossover operations have been tested (e.g., two-point crossover, four-point crossover, etc.). However, only the three-point crossover operation can work for the particular cases probably because the setting of GA's parameters is problem-dependent. Figure 3.19 shows an example of the three-point crossover operation. This operation divides the parent binary individuals into four parts by three random points, respectively, and exchanges the even parts.

Generally, the SAAGA method can successfully recover the GEMTIP parameters for most of the rock samples. It is not absolutely necessary to apply the SAAGA with multipoint crossover operation for all the rock samples because the multipoint crossover operation might increase the computing time. In the following chapter, for the first three rock samples, the GMS method and the SAAGA method will be used to compare the recovered GEMTIP parameters. For the rock samples if the SAAGA method fails to converge, the SAAGA with multipoint crossover operation will be used to compare the inversion results with the GMS method and the SAAGA method.

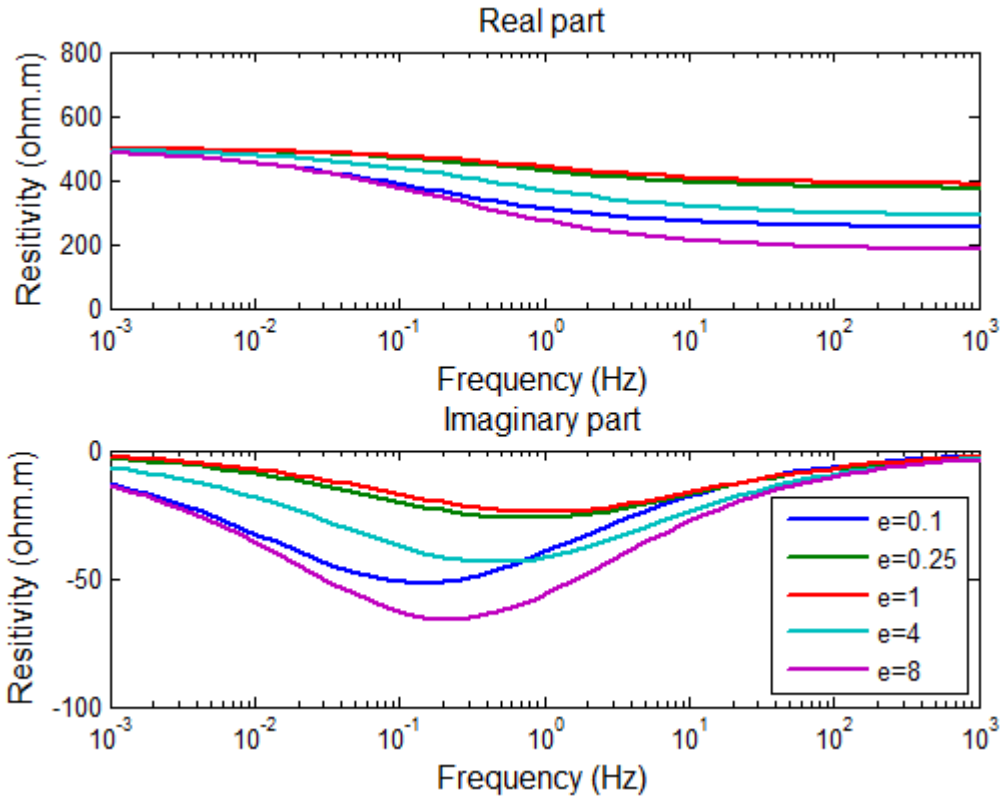

Figure 3.1. Real and imaginary resistivity curves obtained by varying ellipticity (e).

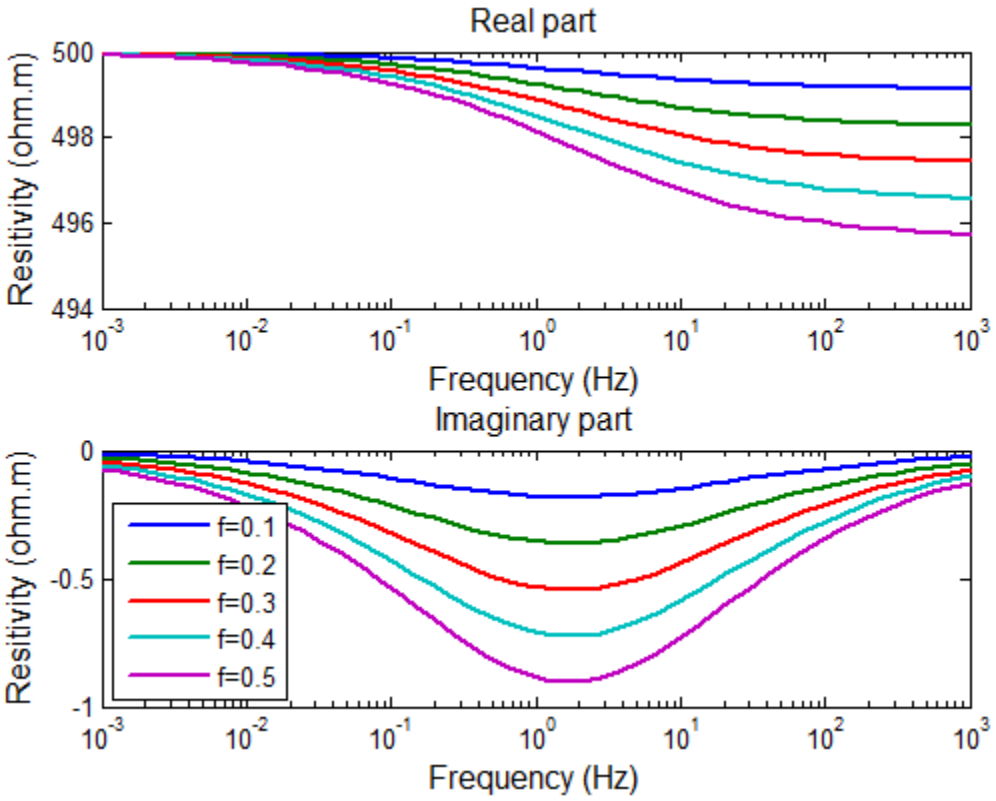

Figure 3.2. Real and imaginary resistivity curves obtained by varying volume fraction (f).

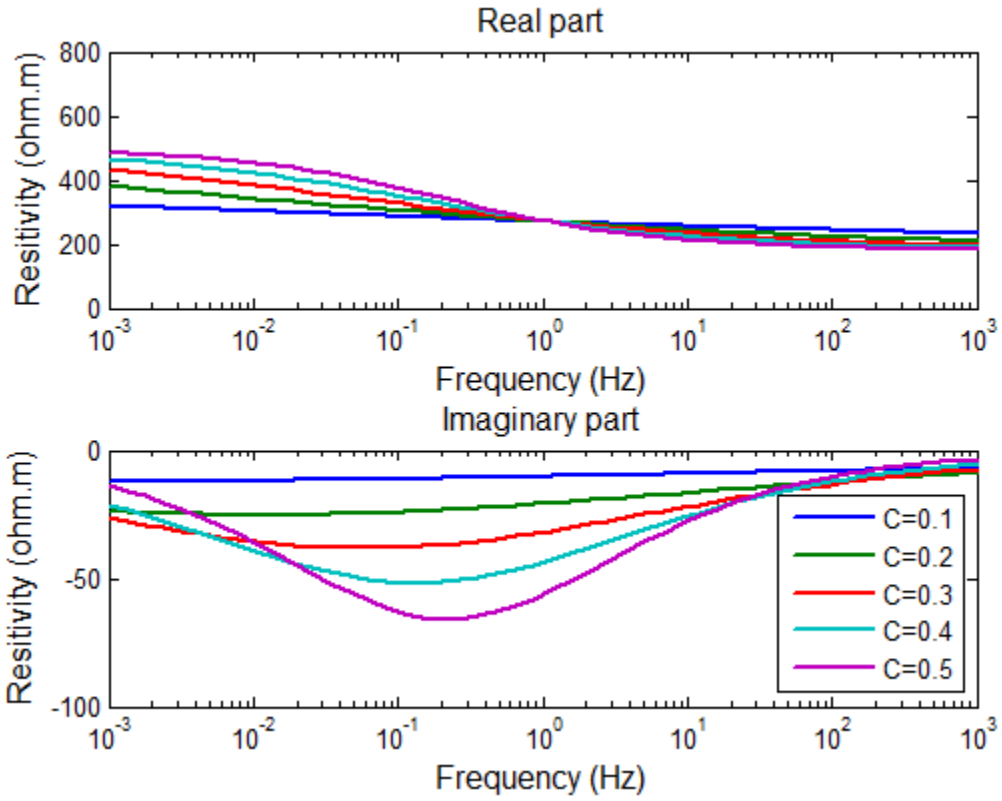

Figure 3.3. Real and imaginary resistivity curves obtained by varying relaxation parameter (C).

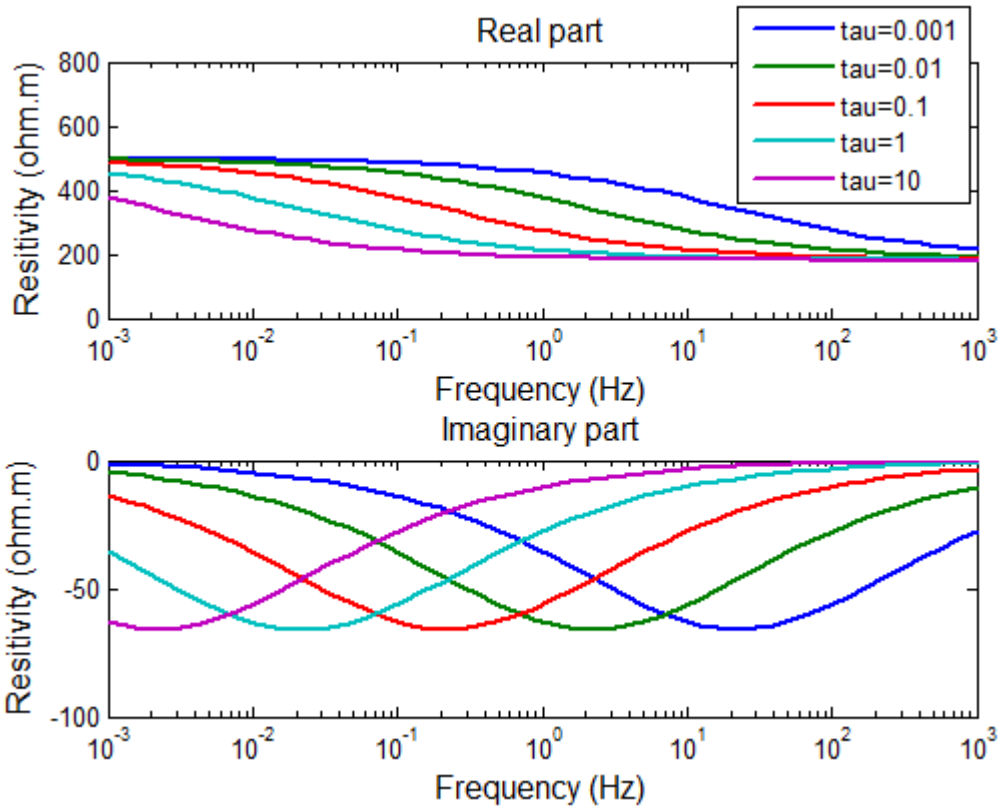

Figure 3.4. Real and imaginary resistivity curves obtained by varying time constant (τ).

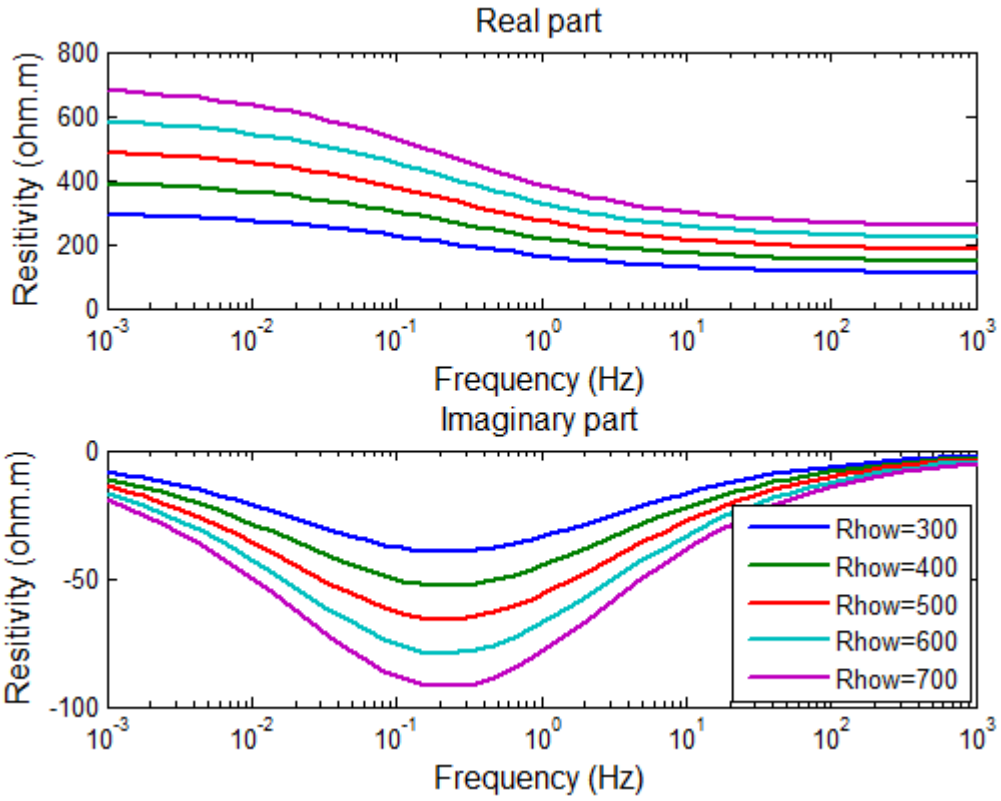

Figure 3.5. Real and imaginary resistivity curves obtained by varying DC resistivity (ρ_0).

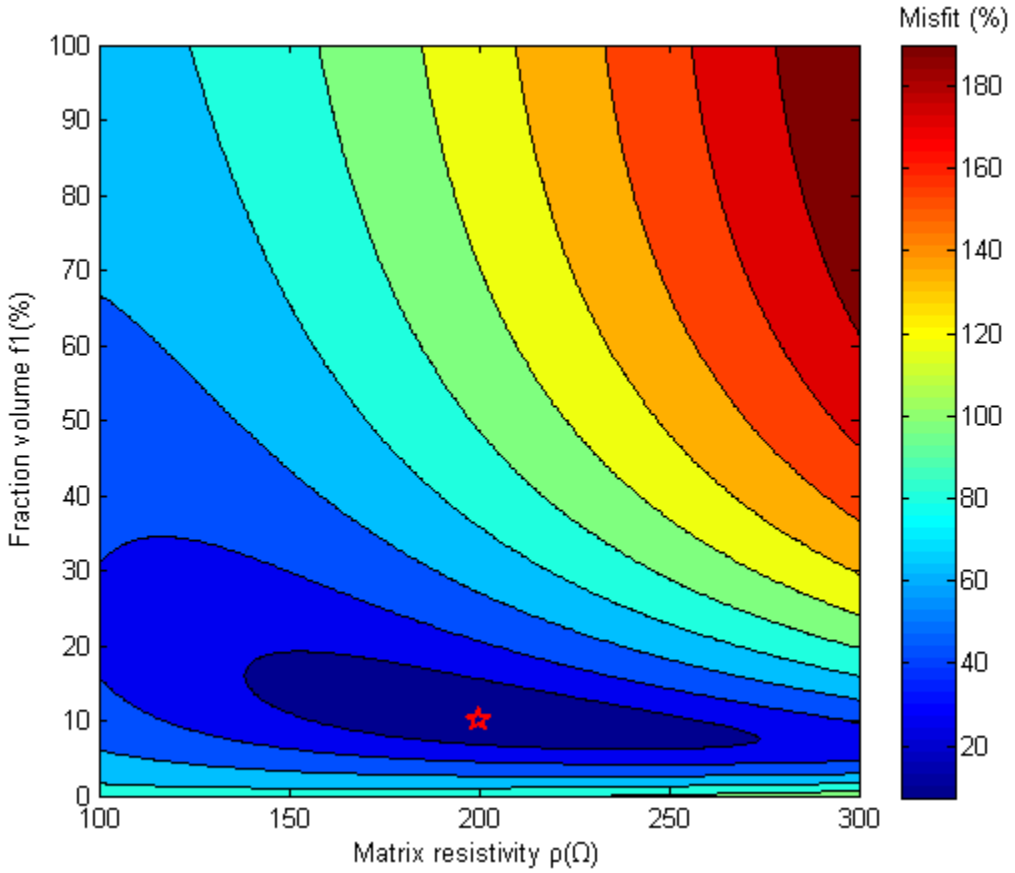

Figure 3.6. Misfit contour map of a three-phase ellipsoidal GEMTIP model.

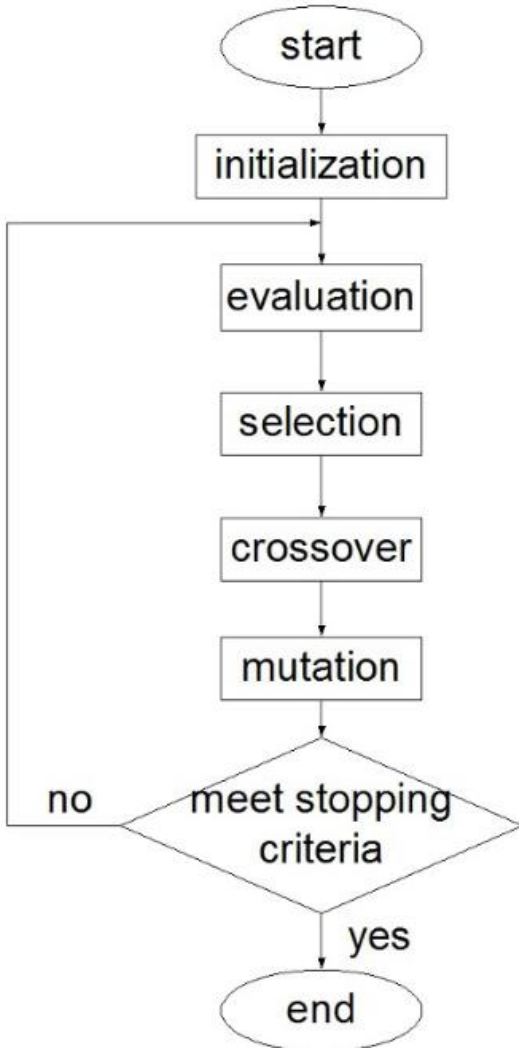

Figure 3.7. The flow chart of the GA method.

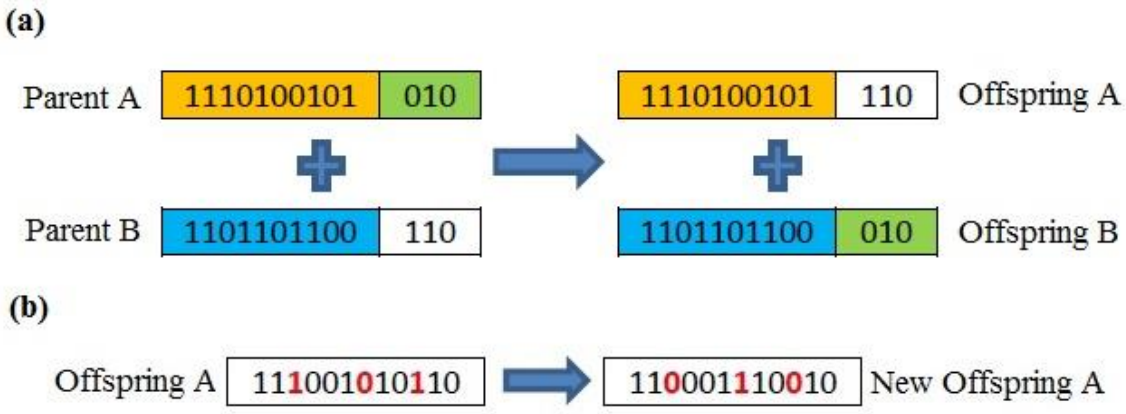

Figure 3.8. Genetic operations. (a) An example of the crossover operation. (b) An example of the mutation operation.

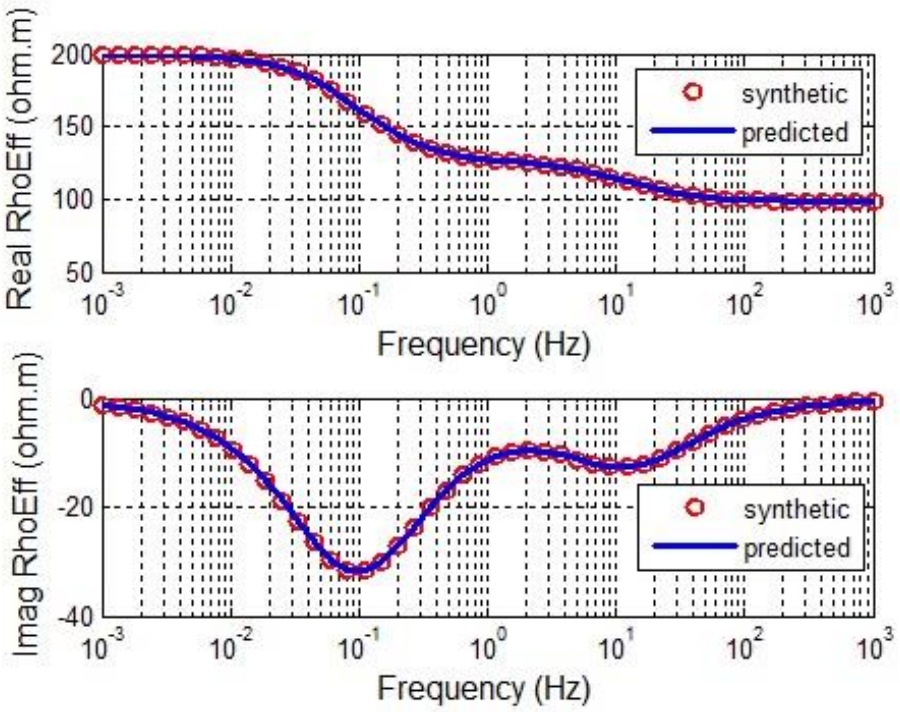

Figure 3.9. Synthetic and predicted CR data computed for the parameters of the GEMTIP model shown in Table 2.3. The top panel shows real part of the CR data, while the bottom panel presents the imaginary CR plots.

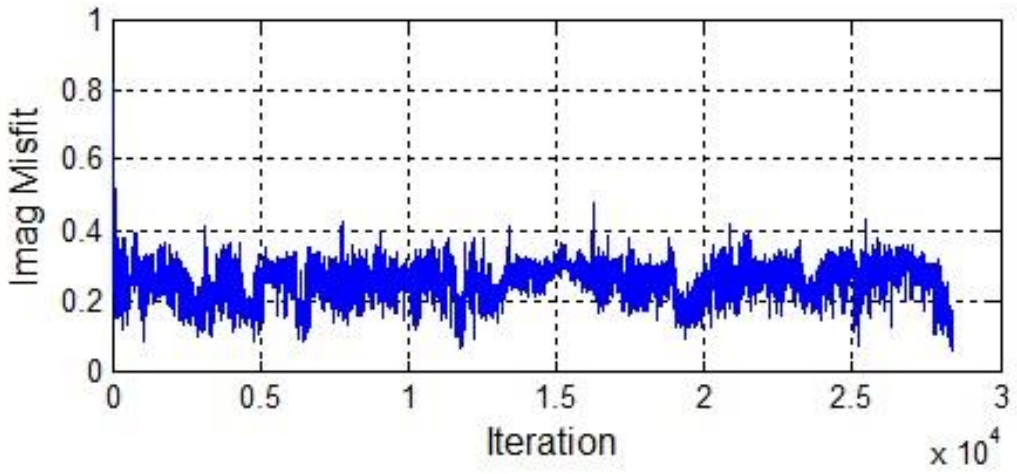

Figure 3.10. The plot of the misfit VS iteration number for the GEMTIP inversion using the GA method.

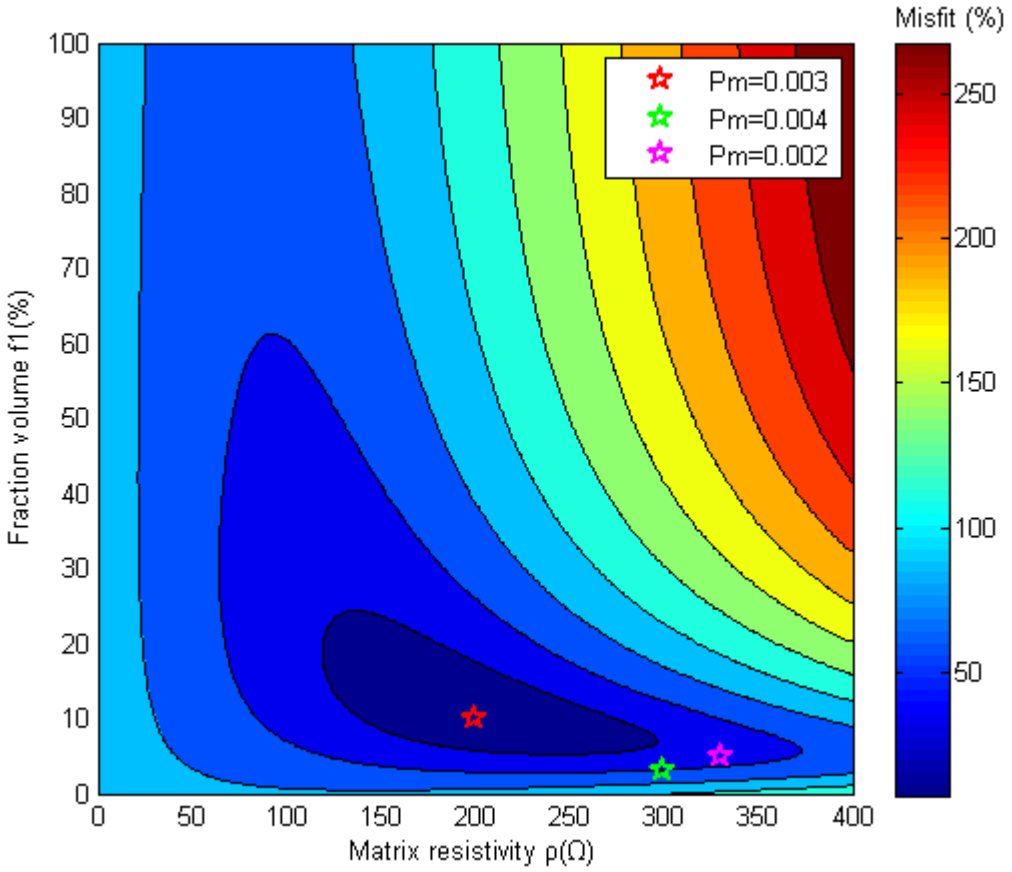

Figure 3.11. Positions of recovered ρ_0 and f_1 for the three cases ($P_m = 0.003$, 0.004 and 0.002) within the misfit contour map.

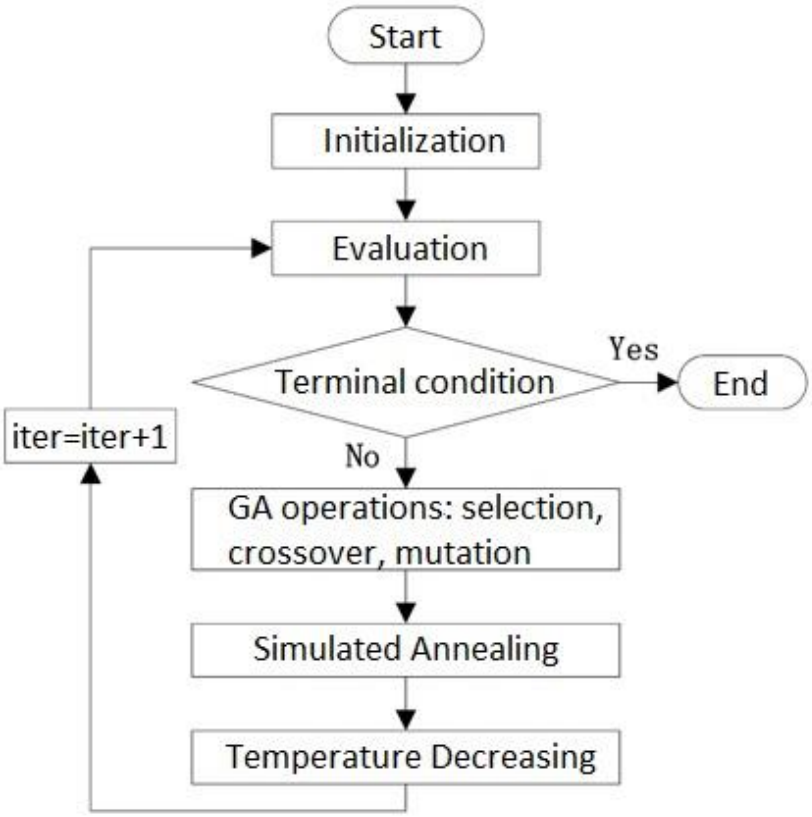

Figure 3.12. Flow chart of the hybrid genetic algorithm with simulated annealing (SAGA).

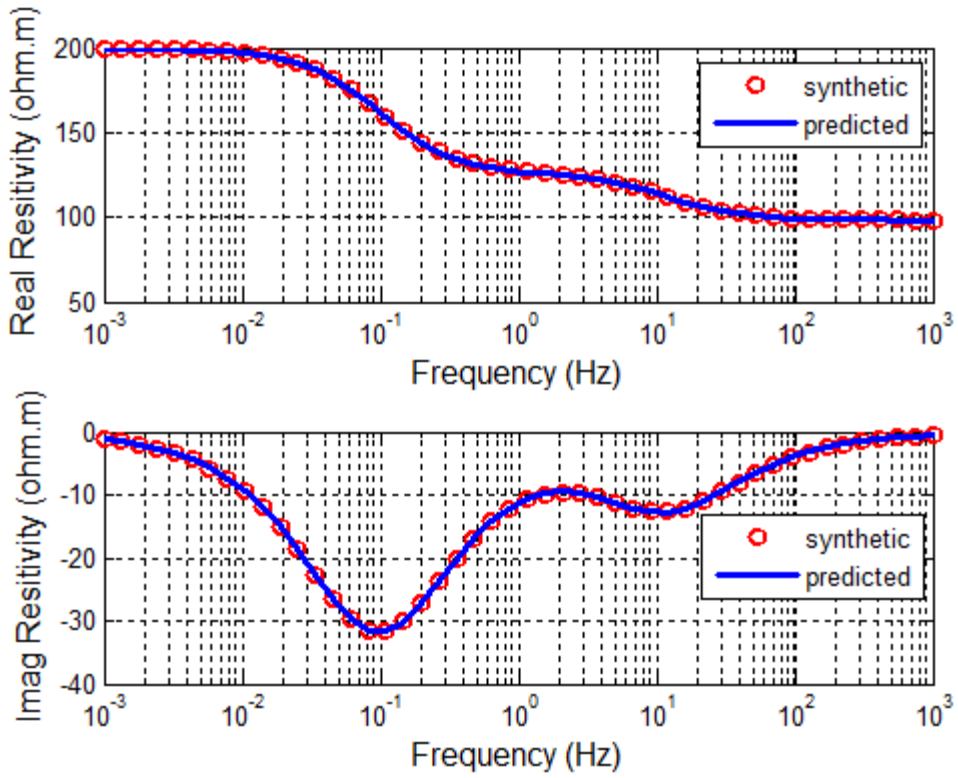

Figure 3.13. Synthetic and predicted CR data computed for case (1). The top panel shows real part of the CR data, while the bottom panel presents the imaginary CR plots.

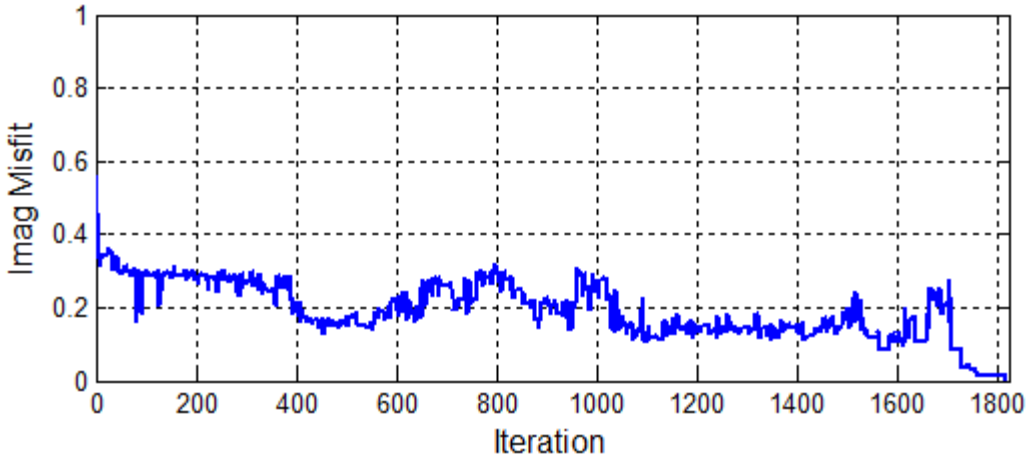

Figure 3.14. The plot of the misfit VS iteration number for GEMTIP inversion using the SAAGA method for case (1).

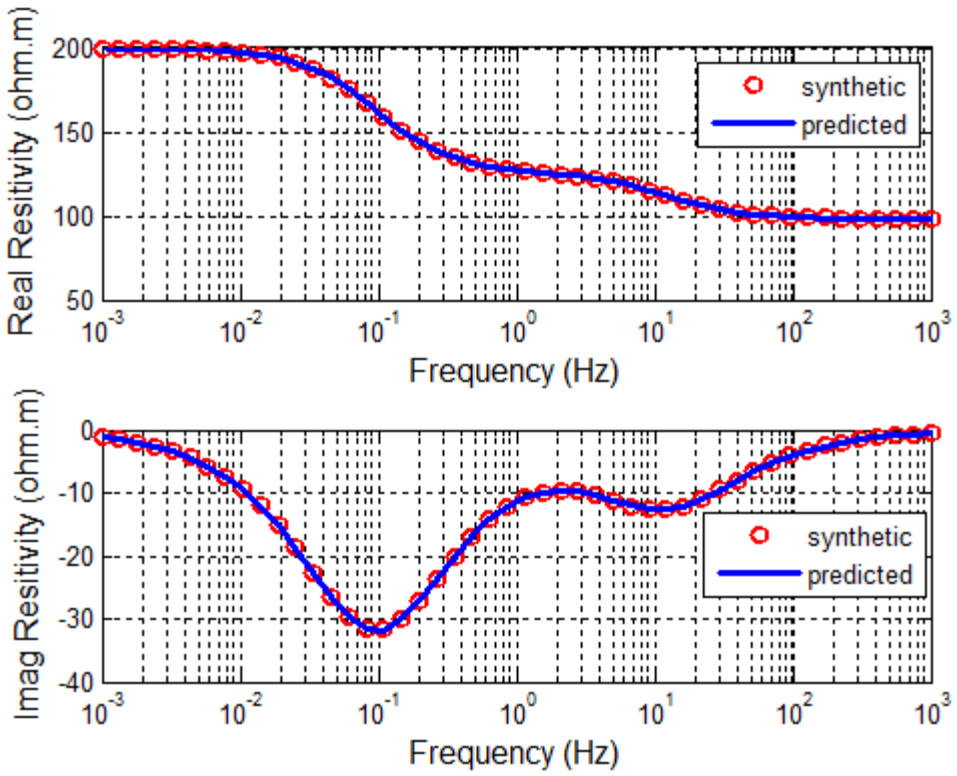

Figure 3.15. Synthetic and predicted CR data computed for case (2). The top panel shows real part of the CR data, while the bottom panel presents the imaginary CR plots.

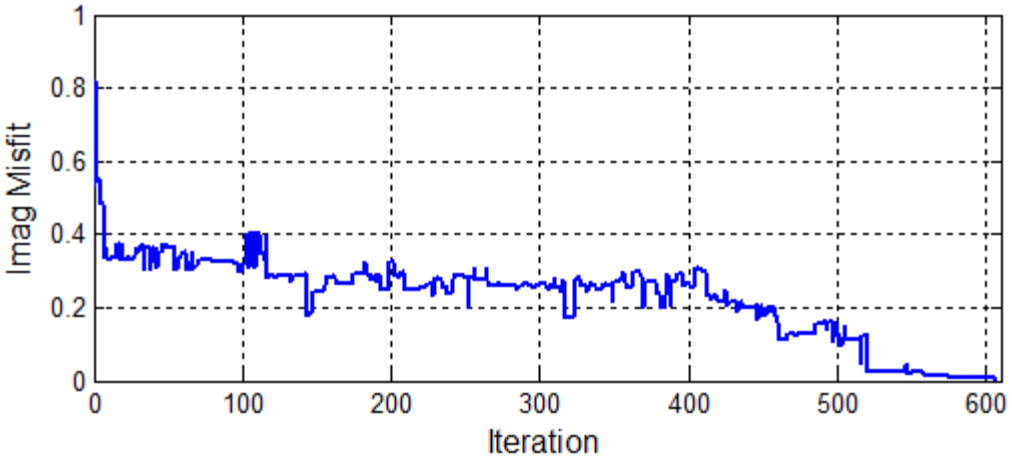

Figure 3.16. The plot of the misfit VS iteration number for GEMTIP inversion using the SAAGA method for case (2).

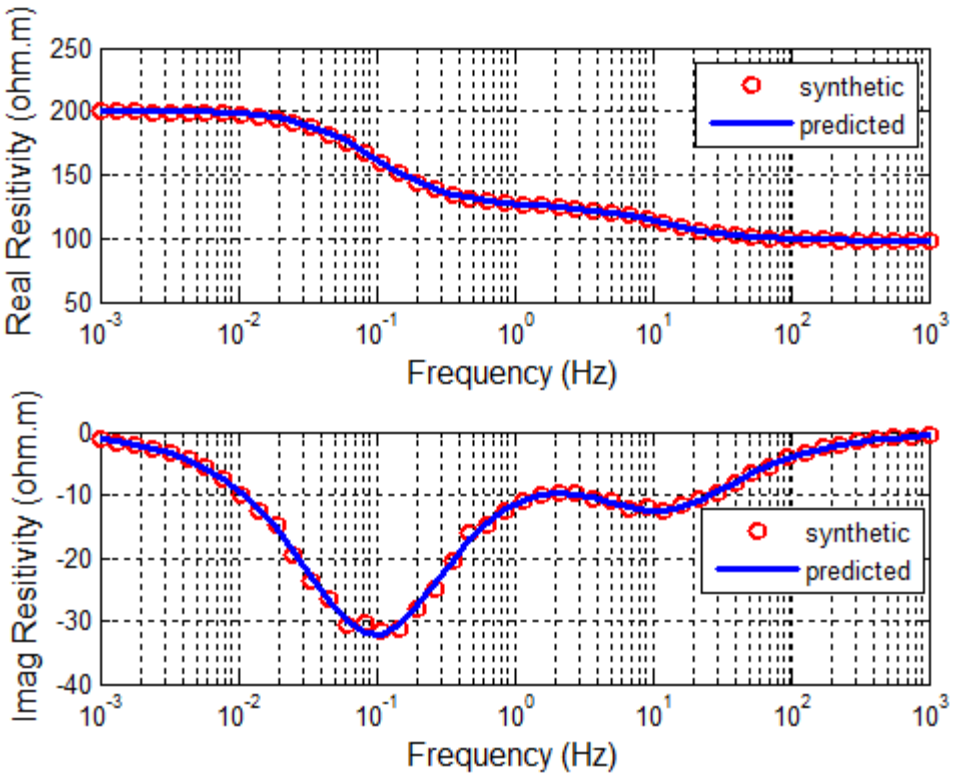

Figure 3.17. Synthetic and predicted CR data computed for case (3). The top panel shows real part of the CR data, while the bottom panel presents the imaginary CR plots.

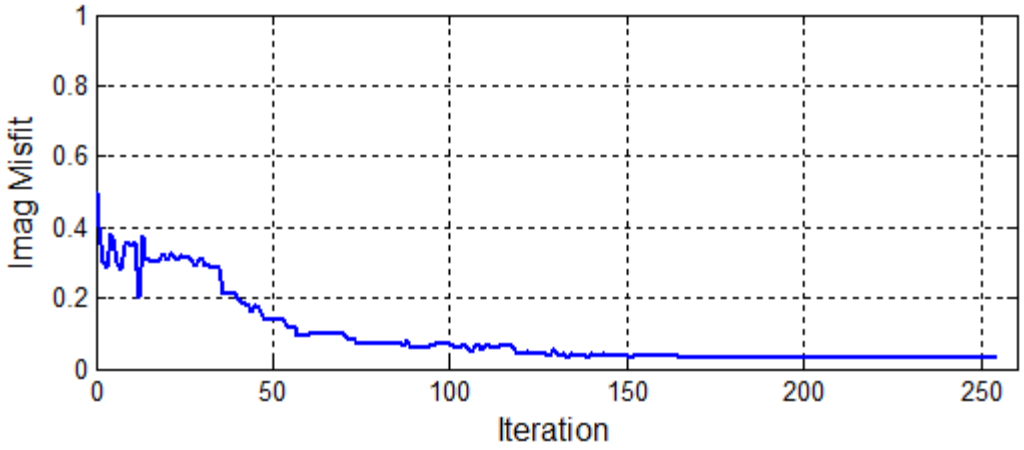

Figure 3.18. The plot of the misfit VS iteration number for GEMTIP inversion using the SAAGA method for case (3).

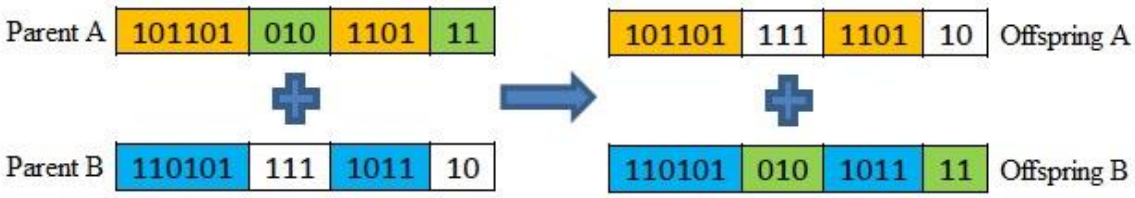

Figure 3.19. An example of the three-point crossover operation.

Table 3.1. Parameters setting of two-phase GEMTIP model varied with ellipticity (e).

Parameter	Value
ρ_0 $(\Omega.m)$	500
τ (s)	0.1
C (-)	0.5
f (%)	10
e (-)	0.1, 0.5, 1, 5, 10

Table 3.2. Parameters setting of two-phase GEMTIP model varied with fraction volume (f).

Parameter	Value
ρ_0 $(\Omega.m)$	500
τ (s)	0.1
C (-)	0.5
e (-)	10
f (%)	10, 20, 30, 40, 50

Table 3.3. Parameters setting of two-phase GEMTIP model varied with relaxation parameter (C).

Parameter	Value
ρ_0 $(\Omega.m)$	500
τ (s)	0.1
f (%)	10
e (-)	10
C (-)	0.1, 0.2, 0.3, 0.4, 0.5

Table 3.4. Parameters setting of two-phase GEMTIP model varied with time constant (τ).

Parameter	Value
ρ_0 $(\Omega.m)$	500
C (-)	0.5
f (%)	10
e (-)	10
τ (s)	0.001, 0.01, 0.1, 1, 10

Table 3.5. Parameters setting of two-phase GEMTIP model varied with DC resistivity (ρ_0).

Parameter	Value
ρ_0 $(\Omega.m)$	300, 400, 500, 600, 700
C (-)	0.5
f (%)	10
e (-)	10
τ (s)	0.1

Table 3.6. An example of the definition of search space and search interval for a synthetic CR data test.

Parameters	True Model	Search space	Number of Segments	Search Interval
$\boldsymbol{\rho_0}$ $(\Omega.m)$	200	[100, 1000]	1024	0.88
$\boldsymbol{e}$ (-)	4	[1, 10]	1024	0.01
$\boldsymbol{\tau}$ (s)	2.0	[0, 10]	1024	0.01
$\boldsymbol{C}$ (-)	0.5	[0, 1]	1024	0.001
$\boldsymbol{f}$ (%)	10	[0, 100]	1024	0.001

Table 3.7. An example of the formation of an individual.

Parameters	$\boldsymbol{\rho_0}$	$\boldsymbol{e_1}$	…	$\boldsymbol{f_2}$
Decimal value	200	2.0	…	10% (0.1)
Binary value	11001000	10	…	0.00011001
Individual	1100100010…000011001			

Table 3.8. Inversion result of the synthetic three-phase ellipsoidal GEMTIP model using the pure genetic algorithm.

Parameters	Synthetic model	Inversion result
$\boldsymbol{\rho_0}$ ($\Omega.m$)	200	200.00
$\boldsymbol{e_1}$ (-)	4	3.94
$\boldsymbol{\tau_1}$ (s)	0.9	0.89
$\boldsymbol{C_1}$ (-)	0.9	0.90
$\boldsymbol{f_1}$ (%)	10	10
$\boldsymbol{e_2}$ (-)	1	1.06
$\boldsymbol{\tau_2}$ (s)	0.01	0.01
$\boldsymbol{C_2}$ (-)	0.9	0.91
$\boldsymbol{f_2}$ (%)	15	15

Table 3.9. Lists of the recovered parameter ρ_0 using three different mutation probabilities.

$P_m = 0.003$		$P_m = 0.004$		$P_m = 0.002$	
Iteration	$\boldsymbol{\rho}_0$	Iteration	$\boldsymbol{\rho}_0$	Iteration	$\boldsymbol{\rho}_0$
24	492.04	505	324.31	505	335.35
25	210.06	506	314.61	506	335.35
26	219.98	507	324.31	507	335.35
27	219.98	508	317.10	508	335.35
28	219.65	509	322.55	509	335.35
29	220.09	510	299.57	510	331.85
30	220.09	511	324.20	511	328.32
31	220.09	512	324.20	512	331.85
32	219.98	513	322.53	513	328.43
33	220.00	514	320.61	514	337.99
34	205.58	515	317.61	515	328.43
35	205.58	516	317.61	516	328.43

Table 3.10. Setting of SA' parameters.

Parameters	Value
T_e	120
λ_T	0.85
VM	5*interval
NS	5
NT	2

Table 3.11. Inversion result of the synthetic three-phase ellipsoidal GEMTIP model using the SAAGA method for case (1).

Parameters	Synthetic model	Inversion result
$\boldsymbol{\rho_0}$ ($\Omega.m$)	200	199.64
$\boldsymbol{e_1}$ (-)	4	4.76
$\boldsymbol{\tau_1}$ (s)	0.9	0.90
$\boldsymbol{C_1}$ (-)	0.9	0.90
$\boldsymbol{f_1}$ (%)	10	8.38
$\boldsymbol{e_2}$ (-)	1	1.38
$\boldsymbol{\tau_2}$ (s)	0.01	0.01
$\boldsymbol{C_2}$ (-)	0.9	0.91
$\boldsymbol{f_2}$ (%)	15	14.36

Table 3.12. Inversion result of the synthetic three-phase ellipsoidal GEMTIP model using the SAAGA method for case (2).

Parameters	Synthetic model	Inversion result
$\boldsymbol{\rho_0}$ ($\Omega.m$)	200	200.23
$\boldsymbol{e_1}$ (-)	4	3.95
$\boldsymbol{\tau_1}$ (s)	0.9	0.91
$\boldsymbol{C_1}$ (-)	0.9	0.90
$\boldsymbol{f_1}$ (%)	10	10.10
$\boldsymbol{e_2}$ (-)	1	1.14
$\boldsymbol{\tau_2}$ (s)	0.01	0.01
$\boldsymbol{C_2}$ (-)	0.9	0.89
$\boldsymbol{f_2}$ (%)	15	15.16

Table 3.13. Inversion result of the synthetic three-phase ellipsoidal GEMTIP model using the SAAGA method for case (3).

Parameters	Synthetic model	Inversion result
$\boldsymbol{\rho_0}$ ($\Omega.m$)	200	201.13
$\boldsymbol{e_1}$ (-)	4	3.70
$\boldsymbol{\tau_1}$ (s)	0.9	0.90
$\boldsymbol{C_1}$ (-)	0.9	0.90
$\boldsymbol{f_1}$ (%)	10	10.83
$\boldsymbol{e_2}$ (-)	1	1.03
$\boldsymbol{\tau_2}$ (s)	0.01	0.01
$\boldsymbol{C_2}$ (-)	0.9	0.88
$\boldsymbol{f_2}$ (%)	15	15.20

CHAPTER 4

CASE STUDIES

This chapter analyzes the experimental data obtained for a representative set of rock samples provided by the CEMI at the University of Utah. The three-phase ellipsoidal GEMTIP model was tested with CR data measured for several typical mineral rock samples. The complex resistivity data were measured over a frequency range from 10^{-2} to 10^{3} Hz at TechnoImaging at Salt Lake City, Utah. In order to decrease the measurement error, all the measured data have been processed by the SMOOTHN function from MATLAB, which provides a fast, automatized, and robust discretized spline smoothing for data of arbitrary dimension. Since the noise of the real effective resistivity is extremely strong, we only consider imaginary part of the complex resistivity for the inversion. These samples have been analyzed by the QEMSCAN system at the Department of Geology and Geophysics, University of Utah. QEMSCAN is a fully-automated micro-analysis system which produces a variety of quantitative parameters of the rock sample including distribution, composition, angularity of minerals, and the fabric, distribution, texture, porosity of materials. The sample description is given below.

4.1 Description of the Rock Samples

4.1.1 Rock Sample #1

Sample #1 is collected from a Cu-Au porphyry deposit. Figure 4.1 is a representative section of this sample produced by the QEMSCAN system. This sample contains 1.48% chalcopyrite, 1.35% pyrite, 0.09% sphalerite, and 0.01% galena. The main two grains in this sample are chalcopyrite and pyrite, which are shown orange and yellow respectively in the representative section.

4.1.2 Rock Sample #2

Sample #2 is also collected from a Carlin-style Au deposit. Figure 4.2 is a representative section of this sample obtained using the QEMSCAN system. This sample contains 58.88% pyrite, 39.96% quartz, 0.83% sulphates, etc. The two main grains in this sample are two different types of pyrite with two different grain sizes. The right figure of panel (a) illustrates some pyrite with big grain sizes concentrated in the upper-left and lower-right areas and some acinose pyrite dispersively distributed in the upper-right and lower-left corners. These two types of pyrite are supposed to have different IP effects.

4.1.3 Rock Sample #3

Sample #3 is another example of a rock from the Carlin-style Au deposit. Figure 4.3 shows a representative section of this sample obtained by the QEMSCAN system. This sample contains 53.97% calcite, 20.45% calcite mixed with quartz, 12.61% quartz, and 2.01% pyrite. The two main grains in this sample are two different types of pyrite with different grain sizes and IP effects. The right figure of panel (a) shows a big piece of pyrite located in the upper area and some small pieces of pyrite distributed in the lower-

left area.

4.1.4 Rock Sample #4

Sample #4 is collected from a Cu-Au porphyry deposit. Figure 4.4 is a representative section of this sample produced by the QEMSCAN system. This sample contains 1.45% chalcopyrite and 0.43% pyrite. The main two grains in this sample are chalcopyrite and pyrite, which are shown orange and yellow respectively in the representative section.

4.1.5 Rock Sample #5

Sample #5 is also collected from a Cu-Au porphyry deposit. Figure 4.5 is a representative section of this sample produced by the QEMSCAN system. This sample contains 0.18% bornite, 0.13% chalcopyrite and 6.64% pyrite. The main two grains in this sample are chalcopyrite and pyrite, which are shown orange and yellow, respectively, in the representative section. In this research, the bornite is considered as it has no IP effect in the measurement.

4.2 Inversion Result of the Rock Samples

This section discusses the inversion results which are based on the hybrid adaptive genetic algorithm with simulated annealing (SAAGA) and global minimum search (GMS) method. The primary purpose is to invert the measured complex resistivity data for specific IP parameters by the three-phase ellipsoidal GEMTIP model. These parameters may be practically used to accurately discriminate minerals or predict useful geometric factors such as matrix resistivity. Additional information on these samples was

extracted using the QEMSCAN as a priori information for the inversion. The inversion recovered parameters are matrix resistivity (ρ_0), ellipticity (e_1 and e_2), time constant (τ_1 and τ_2), relaxation parameter (C_1 and C_2), and volume fraction (f_1 and f_2).

4.2.1 Inversion Result of the Rock Sample #1

The inevitable measurement errors in the observed data may increase the non-uniqueness of the inverse problem using the three-phase ellipsoidal GEMTIP model. To ensure that the inversion result is consistent with the geological explanation (QEMSCAN analysis), in this study, I fixed the volume fraction (percentage of the mineral) of the two grains for both GMS method and SAAGA method.

A previous study of sample #1 used the GMS method to recover the GEMTIP parameters. Figure 4.6 (a) shows the plots of the observed and predicted imaginary part of the CR data. Table 4.1 presents the inversion results for each GEMTIP parameter and the final misfit for the imaginary part of the CR spectrum (2.24%). In this study, the total inversion time was about 5 h.

As in the synthetic example, the hybrid adaptive genetic algorithm with simulated annealing (SAAGA) was also used to recover the GEMTIP model parameters for rock sample #1. Figure 4.6 (b) presents the plots of the observed and predicted imaginary parts of the CR spectrum for sample #1 obtained using SAAGA method. Table 4.2 shows the inversion results for each GEMTIP parameter and the final misfit of the imaginary part of the CR spectrum (1.30%). Compared to the result of the GMS method, the recovered GEMTIP parameters are very close to each other except for the ellipticity. However, the SAAGA method required just about 300 s for the inversion while the inversion time of the GMS method was more than 5 h, and the SAAGA method reached misfit of about 1%

lower than that of the GMS method.

4.2.2 Inversion Result of the Rock Sample #2

For this sample, we know that the total volume fraction of pyrite is 58.88%. So in this study, I fixed the sum of the volume fractions of the two grains during the inversion.

Figure 4.7 (a) shows the plots of the observed and predicted imaginary parts of the CR spectrum for rock sample #2 obtained using the GMS method. Table 4.3 shows the inversion results for different GEMTIP parameters and the final misfit equal to 4.09%. In this study, the total inversion time for the GMS method was about 5 h.

The SAAGA method was applied to recover the GEMTIP parameters for rock sample #2 as well. Figure 4.7 (b) presents the plots of the observed and predicted imaginary parts of the CR spectrum for rock sample #2 obtained using the SAAGA method. Again, the predicted curve fits the observed data very well. Table 4.4 shows the inversion results for every GEMTIP parameters with the final misfit equal to 3.23%. The inversion time for the SAAGA method was about 220 s.

4.2.3 Inversion Result of the Rock Sample #3

Again, in this study I fixed the sum of the volume fractions of the two grains during the inversion to ensure the recovered volume fraction is consistent with the QEMSCAN analysis.

Figure 4.8 (a) shows the observed and predicted curves of the imaginary resistivity obtained by the conventional GMS method. Table 4.5 presents the inversion results and the final misfit equal to 4.18%. In this study, the total inversion time for the GMS method was also about 5 h.

I also applied the novel SAAGA method to recover the GEMTIP variables for sample #3. Figure 3.6 (b) presents the plots of the observed and predicted imaginary parts of the CR spectrum for rock sample #3 obtained using the SAAGA method. Table 4.6 shows the inversion result and the final misfit. Compared to the GMS method, both the computing time (~300 s) and the misfit (3.50%) are much smaller than those of the GMS method, which demonstrate the advantages of the SAAGA method.

4.2.4 Inversion Result of the Rock Sample #4

For this sample, we know that the volume fractions of the minerals are 1.45% (chalcopyrite) and 0.43% (pyrite), respectively. So in this study, I fixed the volume fractions of the two grains during the inversion.

A previous study of sample #4 used the GMS method to recover the GEMTIP parameters. Figure 4.9 (a) shows the plots of the observed and predicted imaginary part of the CR data. Table 4.7 presents the inversion results for each GEMTIP parameter and the final misfit for the imaginary part of the CR spectrum (7.41%). According the observed CR data, it is clear that the peak of IP effect is very flat which is unusual from the previous rock samples, probably because the peaks of IP effect of the two grains are overlapped in this area. Besides, the high misfit of the inversion result by using the GMS method indicates that the inverse problem of this sample may not be as successful as the previous samples.

The SAAGA method was applied to this rock sample. However, the inversion result cannot converge and the misfit is always larger than 10% probably due to the complicated observed CR curve. Since there are thousands of solutions which might have approximate 10% misfit, it is not possible to show the inversion result of the SAAGA

method. Thus, the SAAGA method cannot work for this case.

The SAAGA with multipoint crossover operation was also used to recover the GEMTIP model parameters for rock sample #4. Figure 4.9 (b) presents the plots of the observed and predicted imaginary parts of the CR spectrum for sample #4 obtained using the SAAGA with multipoint crossover operation. Table 4.8 shows the inversion results for each GEMTIP parameter and the final misfit of the imaginary part of the CR spectrum (6.52%). Compared to the GMS method, the misfit of the SAAGA with multipoint crossover operation is about 1% lower. The total computing time is about 7 minutes.

4.2.5 Inversion Result of the Rock Sample #5

For this sample, we know that the volume fractions of chalcopyrite and pyrite are 0.13% and 6.64%, respectively. So in this study, I fixed the volume fractions of the two grains during the inversion.

A previous study of sample #5 used the GMS method to recover the GEMTIP parameters. Figure 4.10 (a) shows the plots of the observed and predicted imaginary part of the CR data. Table 4.9 presents the inversion results for each GEMTIP parameter and the final misfit for the imaginary part of the CR spectrum (6.71%). The unusual observed CR curve shows that the CR data gradually increase with the frequencies. We can assume the peak of IP effect might be in a very low frequency area (e.g., 10^{-3}Hz). According to the previous chapter, we know the main factors which affect the position of the peak are time constant (τ) and ellipticity (e). Higher τ and higher e will shift the peak of IP effect into low-frequency area. Thus, these two parameters of this rock sample might be very close to the bound of the search area, which might increase the difficulty of the inversion. The high misfit of the inversion result of the GMS method also proves that the inverse

problem of this sample is very challenging.

The SAAGA method was applied to this rock sample. Figure 4.10 (b) presents the plots of the observed and predicted imaginary parts of the CR spectrum for sample #5 obtained using SAAGA method. Table 4.10 shows the inversion results for each GEMTIP parameter and the final misfit of the imaginary part of the CR spectrum (8.45%). And the computing time is about 10 minutes. However, compared to the GMS method, the SAAGA with multipoint crossover operation reached misfit of about 2% higher, which means the SAAGA method failed to recover the GEMTIP parameters for this case.

The SAAGA with multipoint crossover operation was also used to recover the GEMTIP model parameters for rock sample #5. Figure 4.10 (c) presents the plots of the observed and predicted imaginary parts of the CR spectrum for sample #5 obtained using the SAAGA with multipoint crossover operation. Table 4.11 shows the inversion results for each GEMTIP parameter and the final misfit of the imaginary part of the CR spectrum (4.30%). The computing time for this method is about 5 minutes. Compared to the GMS method and the SAAGA method, the SAAGA with multipoint crossover operation reached a very low misfit which is about 2% and 4% lower, respectively. Obviously, the predicted CR curve fits much better than previous inversion results. According to the recovered parameters, we can find that the time constant (τ_1) is 9.29 and the ellipticity (e_2) is 9.63, which is consistent with the previous assumption.

4.3 Discussion

Totally five rock samples were analyzed using the three-phase ellipsoidal GEMTIP model. I have developed a method of minimizing the objective functional using the hybrid adaptive genetic algorithm with simulated annealing (SAAGA), which

provides a novel and feasible approach to interpret the pertrophysical properties from the observed CR data using the three-phase ellipsoidal GEMTIP model. It has the following advantages over the global minimum search (GMS) method: First, while the GMS method takes a significantly long searching time to meet a termination condition, the SAAGA method only needs several minutes to find a solution which has a lower misfit than that of the GMS method. With larger search spaces and smaller intervals, this fact would obviously be amplified. Second, because the search interval of each GEMTIP parameter is much smaller, the recovered parameters of the SAAGA method are more accurate compared with the inversion results of the GMS method. However, limitation does exist. The measurement errors of the observed CR data increase the nonuniqueness and instability of the inverse problem. In order to make the recovered GEMTIP parameters to be consistent with the geological interpretation (e.g., QEMSCAN analysis), the volume fraction is fixed to constrain the inversion result.

Besides, in order to recover the GEMTIP parameters for some rock samples which have complicated observed CR data, a modified hybrid genetic algorithm have been developed based on the hybrid adaptive genetic algorithm with simulated annealing (SAAGA) and multipoint crossover operation. Two rock samples were analyzed using the three-phase ellipsoidal GEMTIP model by the GMS method, the SAAGA method and the SAAGA with multipoint crossover operation respectively. According to the inversion results of the case studies, the final misfits of the GMS method and the SAAGA method are extremely high, even the SAAGA method cannot converge in the rock sample #4. However, the SAAGA with multipoint crossover operation successfully recovered the GEMTIP parameters and got lower misfits without losing the efficiency.

In summary, the SAAGA method is effective and fast for the GEMTIP inversion

of most of the rock samples. For those rock samples when the SAAGA method fails to recover the GEMTIP parameters, the SAAGA with multipoint crossover operation is an alternative method for the inverse problem of the three-phase GEMTIP model. The experience of this research illustrates that this algorithm provides a possible solution for the nonlinear geophysical inverse problem with high nonuniqueness and instability.

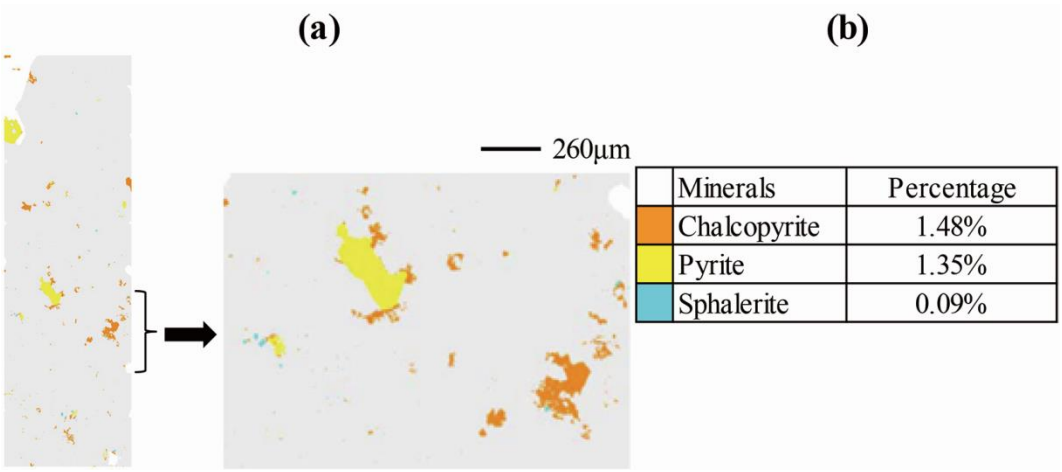

Figure 4.1. A representative section of rock sample #1 produced by the QEMSCAN system. Panel (a) shows the entire image of the analyzed section. Panel (b) presents the names and % of the corresponding minerals.

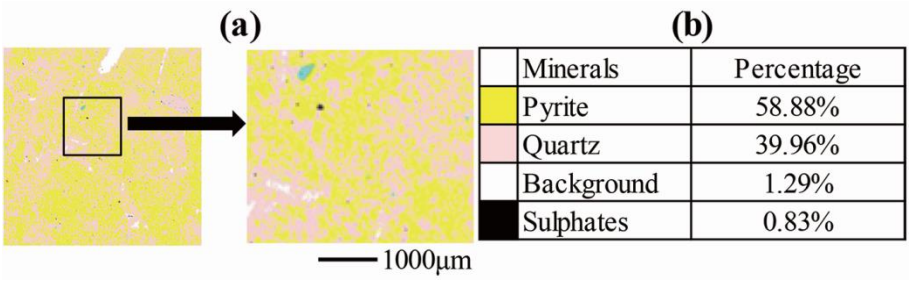

Figure 4.2. A representative section of rock sample #2 produced by the QEMSCAN system. Panel (a) shows the entire image of the analyzed section. Panel (b) presents the names and % of the corresponding minerals.

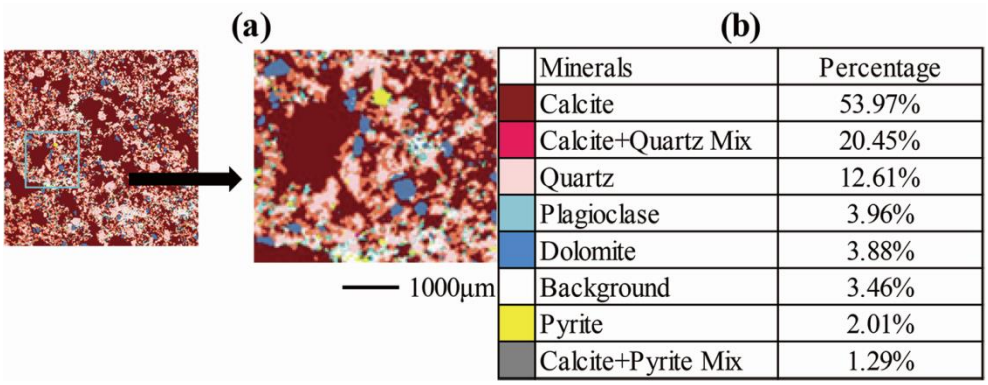

	Minerals	Percentage
	Calcite	53.97%
	Calcite+Quartz Mix	20.45%
	Quartz	12.61%
	Plagioclase	3.96%
	Dolomite	3.88%
	Background	3.46%
	Pyrite	2.01%
	Calcite+Pyrite Mix	1.29%

Figure 4.3. A representative section of rock sample #3 produced by the QEMSCAN system. Panel (a) shows the entire image of the analyzed section. Panel (b) presents the names and % of the corresponding minerals.

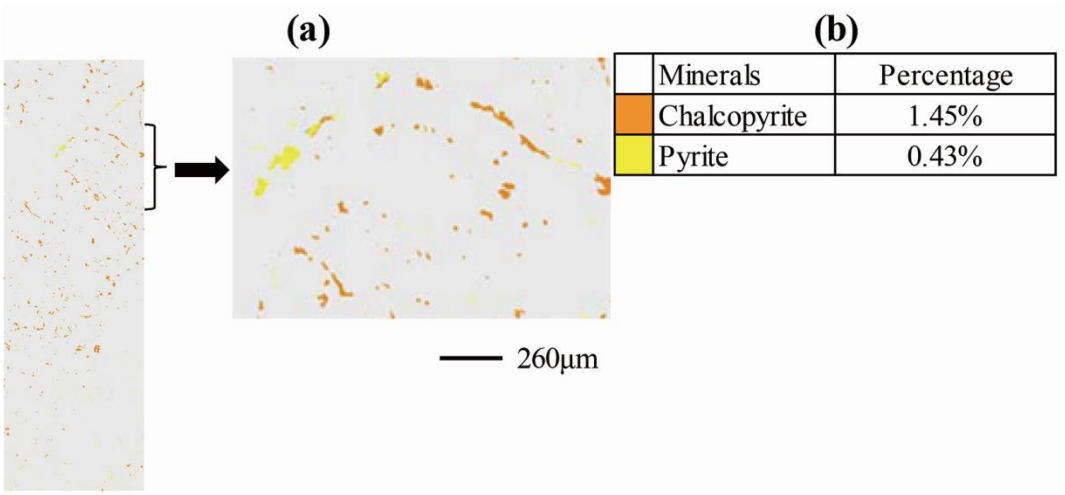

Figure 4.4. A representative section of rock sample #4 produced by the QEMSCAN system. Panel (a) shows the entire image of the analyzed section. Panel (b) presents the names and % of the corresponding minerals.

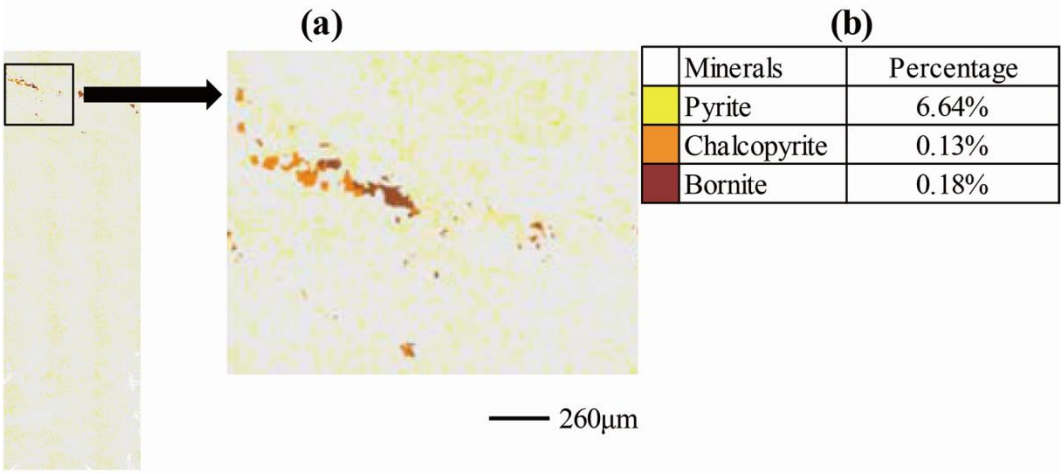

Figure 4.5. A representative section of rock sample #5 produced by the QEMSCAN system. Panel (a) shows the entire image of the analyzed section. Panel (b) presents the names and % of the corresponding minerals.

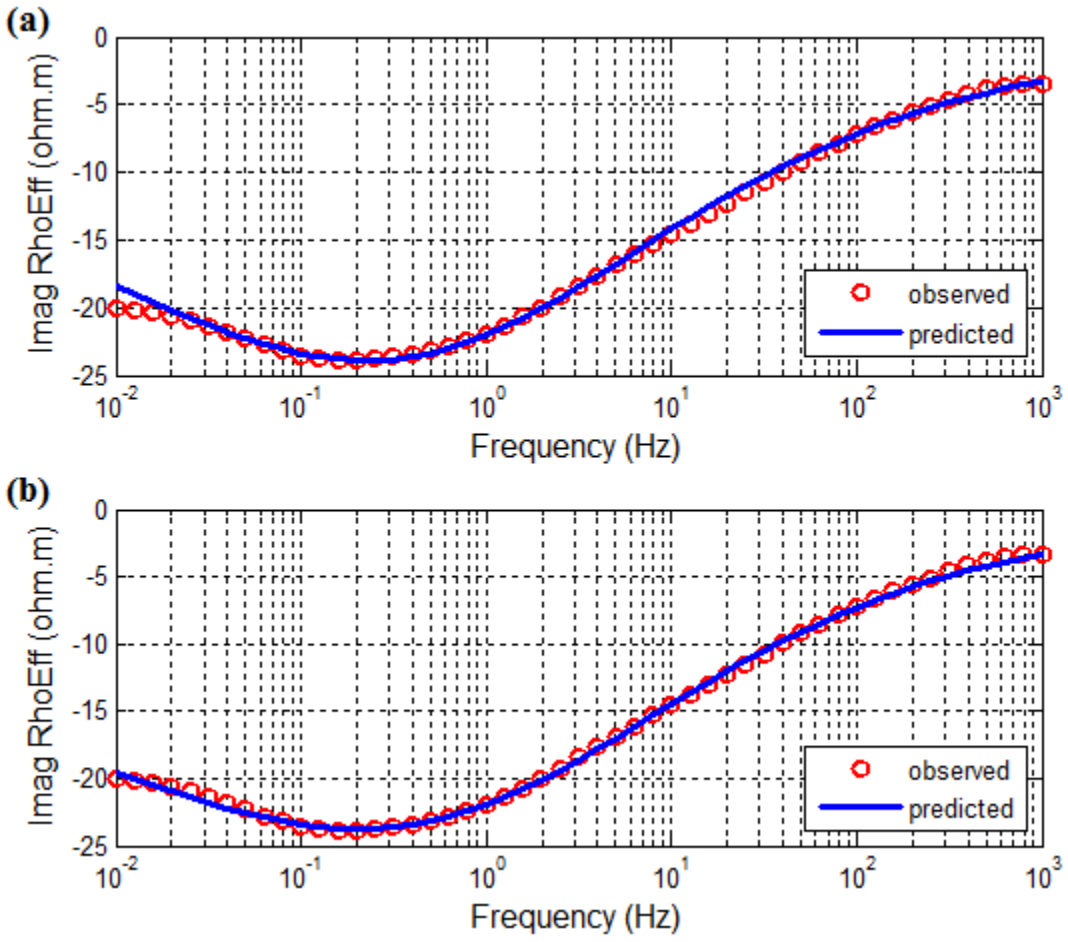

Figure 4.6. Inversion results of rock sample #1. (a) Plots of the observed and predicted imaginary parts of the CR spectrum obtained using the GMS method. (b) Plots of the observed and predicted imaginary parts of the CR spectrum obtained using the SAAGA method.

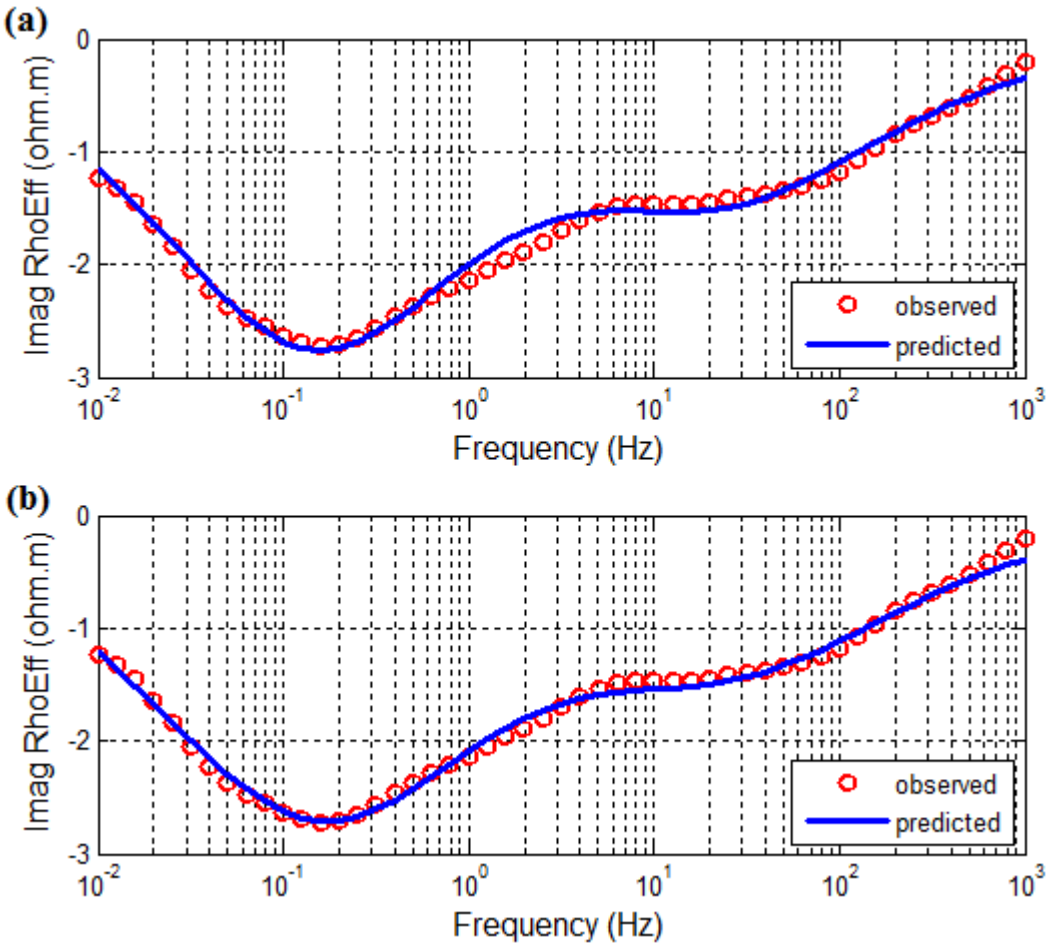

Figure 4.7. Inversion results of rock sample #2. (a) Plots of the observed and predicted imaginary parts of the CR spectrum obtained using the GMS method. (b) Plots of the observed and predicted imaginary parts of the CR spectrum obtained using the SAAGA method.

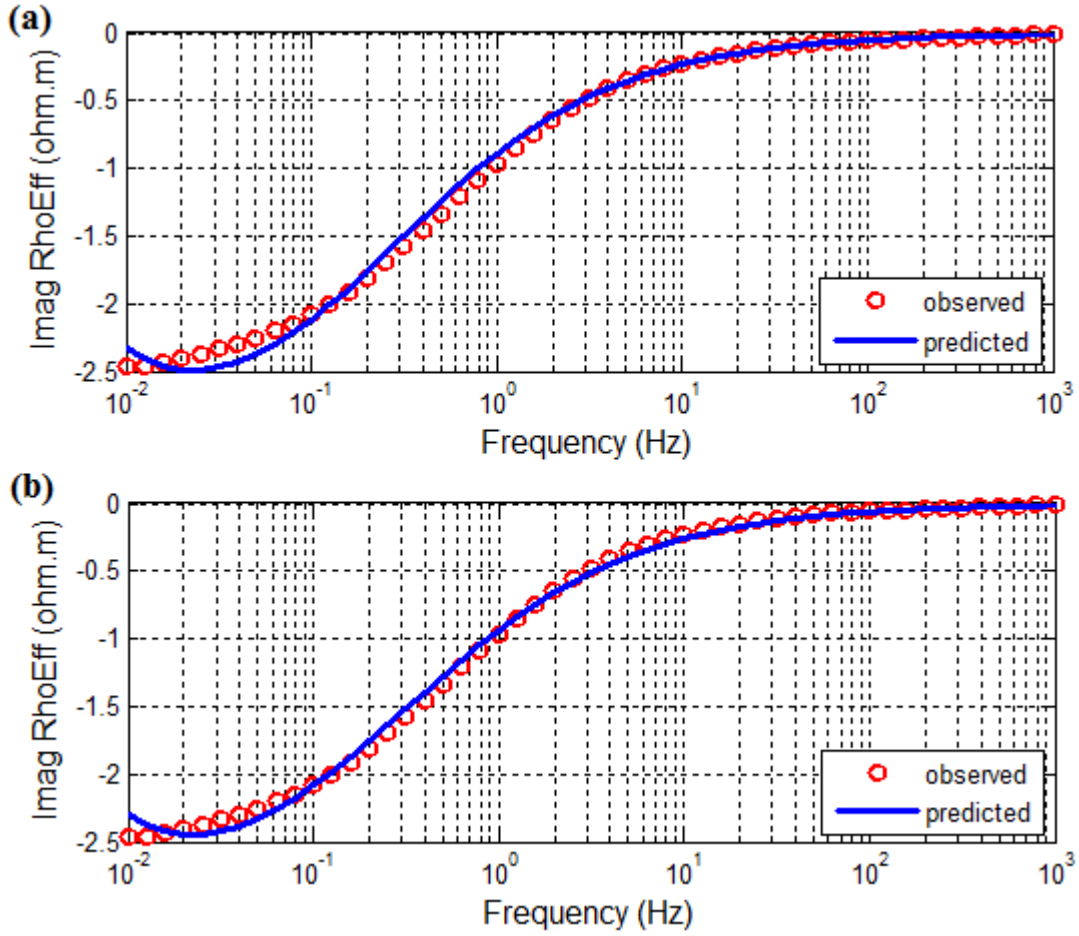

Figure 4.8. Inversion results of rock sample #3. (a) Plots of the observed and predicted imaginary parts of the CR spectrum obtained using the GMS method. (b) Plots of the observed and predicted imaginary parts of the CR spectrum obtained using the SAAGA method.

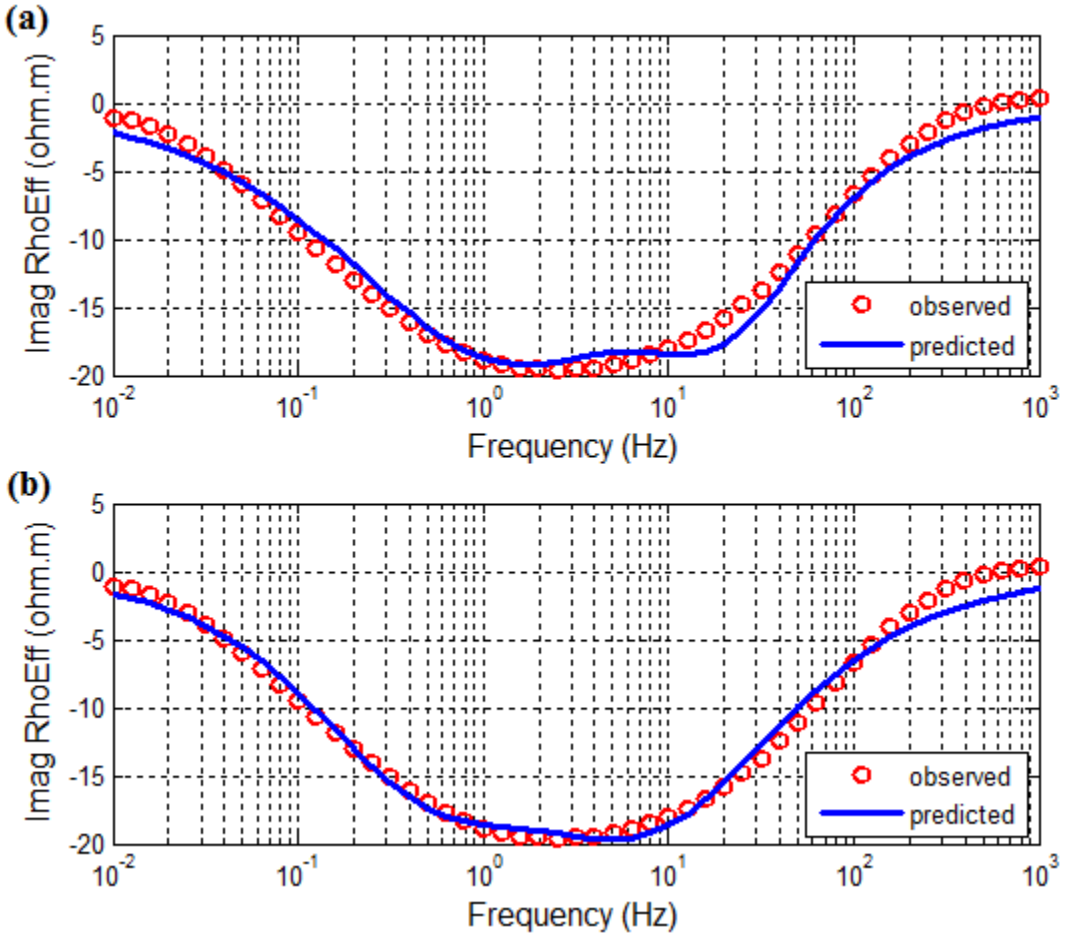

Figure 4.9. Inversion results of rock sample #4. (a) Plots of the observed and predicted imaginary parts of the CR spectrum obtained using the GMS method. (b) Plots of the observed and predicted imaginary parts of the CR spectrum obtained using the SAAGA with multipoint crossover operation.

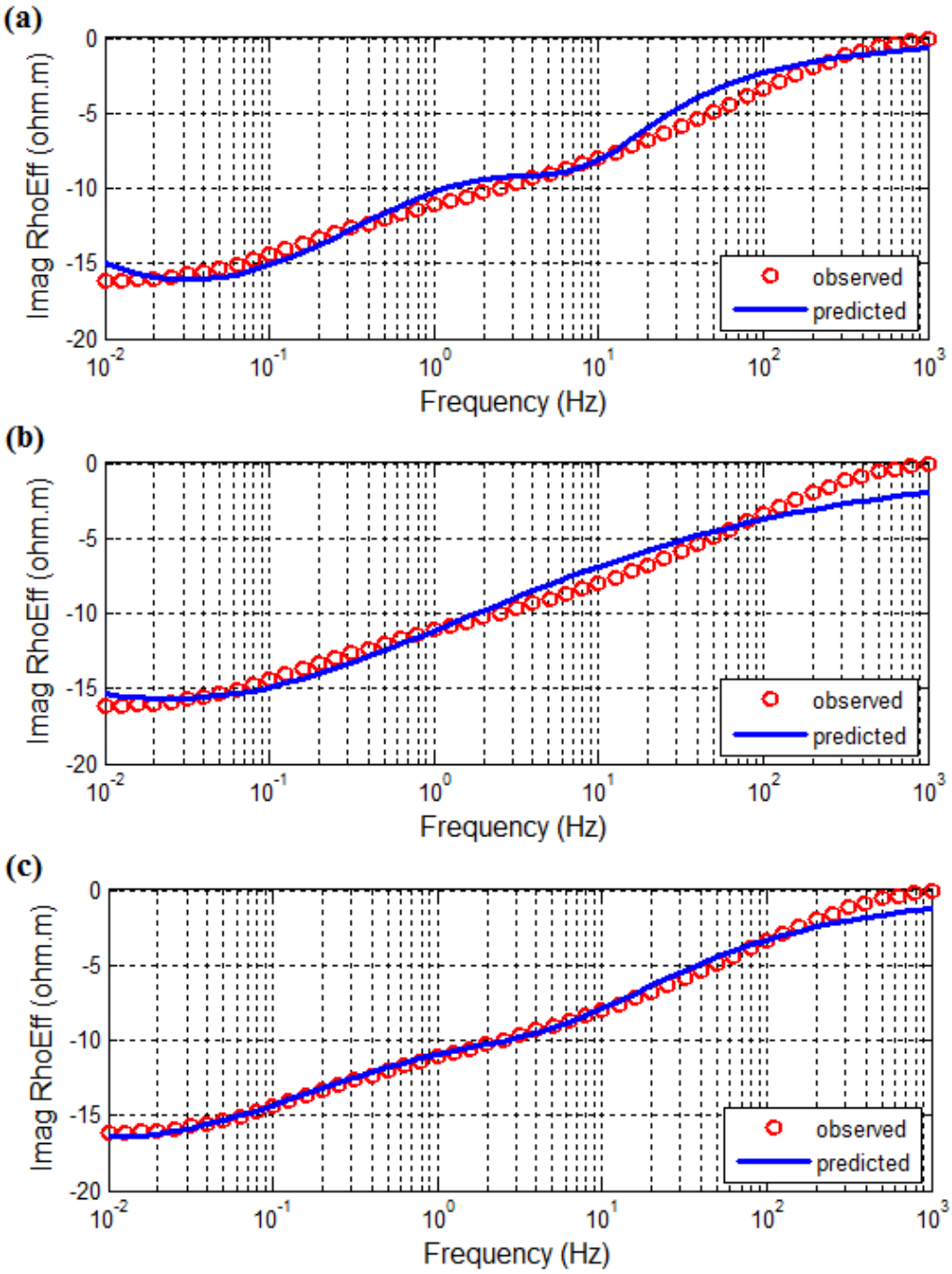

Figure 4.10. Inversion results of rock sample #5. (a) Plots of the observed and predicted imaginary parts of the CR spectrum obtained using the GMS method. (b) Plots of the observed and predicted imaginary parts of the CR spectrum obtained using the SAAGA method. (c) Plots of the observed and predicted imaginary parts of the CR spectrum obtained using the SAAGA with multipoint crossover operation.

Table 4.1. GEMTIP inversion results for rock sample #1 obtained using the GMS method.

Misfit		2.24%	
$\rho_0(\Omega.m)$		1931	
Grain 1: Pyrite		Grain 2: Chalcopyrite	
Ellipticity e_1 (-)	2.5	Ellipticity e_2 (-)	1.6
Time Constant $\tau_1(s)$	0.28	Time Constant $\tau_2(s)$	10
Relaxation coefficient C_1 (-)	0.43	Relaxation coefficient C_2 (-)	0.28
Fraction volume $f_1(\%)$	1.35	Fraction volume $f_2(\%)$	1.48

Table 4.2. GEMTIP inversion results for rock sample #1 obtained using the SAAGA method.

Misfit		1.30%	
$\rho_0(\Omega.m)$		1959	
Grain 1: Pyrite		Grain 2: Chalcopyrite	
Ellipticity e_1 (-)	1.75	Ellipticity e_2 (-)	2.58
Time Constant $\tau_1(s)$	0.20	Time Constant $\tau_2(s)$	8.81
Relaxation coefficient C_1 (-)	0.44	Relaxation coefficient C_2 (-)	0.30
Fraction volume $f_1(\%)$	1.35	Fraction volume $f_2(\%)$	1.48

Table 4.3. GEMTIP inversion results for rock sample #2 obtained using the GMS method.

Misfit		4.09%	
$\rho_0(\Omega.m)$		19	
Grain 1: Pyrite 1		Grain 2: Pyrite 2	
Ellipticity e_1 (-)	4.0	Ellipticity e_2 (-)	1.0
Time Constant $\tau_1(s)$	0.002	Time Constant $\tau_2(s)$	0.41
Relaxation coefficient C_1 (-)	0.66	Relaxation coefficient C_2 (-)	0.66
Fraction volume $f_1(\%)$	28	Fraction volume $f_2(\%)$	30

Table 4.4. GEMTIP inversion results for rock sample #2 obtained using the SAAGA method.

Misfit		3.23%	
$\rho_0(\Omega.m)$		21	
Grain 1: Pyrite 1		Grain 2: Pyrite 2	
Ellipticity e_1 (-)	2.44	Ellipticity e_2 (-)	1.24
Time Constant $\tau_1(s)$	0.002	Time Constant $\tau_2(s)$	0.39
Relaxation coefficient C_1 (-)	0.62	Relaxation coefficient C_2 (-)	0.62
Fraction volume $f_1(\%)$	31.79	Fraction volume $f_2(\%)$	27.07

Table 4.5. GEMTIP inversion results for rock sample #3 obtained using the GMS method.

Misfit		4.18%	
$\rho_0(\Omega.m)$		72	
Grain 1: Pyrite 1		Grain 2: Pyrite 2	
Ellipticity e_1 (-)	10.0	Ellipticity e_2 (-)	4.0
Time Constant $\tau_1(s)$	1.35	Time Constant $\tau_2(s)$	10.0
Relaxation coefficient C_1 (-)	0.66	Relaxation coefficient C_2 (-)	0.66
Fraction volume $f_1(\%)$	0.4	Fraction volume $f_2(\%)$	1.61

Table 4.6. GEMTIP inversion results for rock sample #3 obtained using the SAAGA method.

Misfit		3.50%	
$\rho_0(\Omega.m)$		70.47	
Grain 1: Pyrite 1		Grain 2: Pyrite 2	
Ellipticity e_1 (-)	8.52	Ellipticity e_2 (-)	4.65
Time Constant $\tau_1(s)$	1.00	Time Constant $\tau_2(s)$	8.86
Relaxation coefficient C_1 (-)	0.64	Relaxation coefficient C_2 (-)	0.64
Fraction volume $f_1(\%)$	0.45	Fraction volume $f_2(\%)$	1.56

Table 4.7. GEMTIP inversion results for rock sample #4 obtained using the GMS method.

Misfit		7.41%	
$\rho_0(\Omega.m)$		1389	
Grain 1: Pyrite		Grain 2: Chalcopyrite	
Ellipticity e_1 (-)	2.5	Ellipticity e_2 (-)	1.6
Time Constant $\tau_1(s)$	0.007	Time Constant $\tau_2(s)$	0.12
Relaxation coefficient C_1 (-)	1	Relaxation coefficient C_2 (-)	0.66
Fraction volume $f_1(\%)$	0.43	Fraction volume $f_2(\%)$	1.45

Table 4.8. GEMTIP inversion results for rock sample #4 obtained using the SAAGA with multipoint crossover operation.

Misfit		6.52%	
$\rho_0(\Omega.m)$		1015.08	
Grain 1: Pyrite		Grain 2: Chalcopyrite	
Ellipticity e_1 (-)	5.38	Ellipticity e_2 (-)	2.21
Time Constant $\tau_1(s)$	0.29	Time Constant $\tau_2(s)$	0.02
Relaxation coefficient C_1 (-)	0.82	Relaxation coefficient C_2 (-)	0.75
Fraction volume $f_1(\%)$	0.43	Fraction volume $f_2(\%)$	1.45

Table 4.9. GEMTIP inversion results for rock sample #5 obtained using the GMS method.

Misfit		6.71%	
$\rho_0(\Omega.m)$		518	
Grain 1: Pyrite		Grain 2: Chalcopyrite	
Ellipticity e_1 (-)	1.6	Ellipticity e_2 (-)	10
Time Constant $\tau_1(s)$	3.01	Time Constant $\tau_2(s)$	0.02
Relaxation coefficient C_1 (-)	0.43	Relaxation coefficient C_2 (-)	1
Fraction volume $f_1(\%)$	6.64	Fraction volume $f_2(\%)$	0.13

Table 4.10. GEMTIP inversion results for rock sample #5 obtained using the SAAGA method.

Misfit		8.45%	
$\rho_0(\Omega.m)$		713	
Grain 1: Pyrite		Grain 2: Chalcopyrite	
Ellipticity e_1 (-)	1.04	Ellipticity e_2 (-)	4.75
Time Constant $\tau_1(s)$	3.89	Time Constant $\tau_2(s)$	0.19
Relaxation coefficient C_1 (-)	0.32	Relaxation coefficient C_2 (-)	0.33
Fraction volume $f_1(\%)$	6.64	Fraction volume $f_2(\%)$	0.14

Table 4.11. GEMTIP inversion results for rock sample #5 obtained using the SAAGA with multipoint crossover operation.

Misfit		4.30%	
$\rho_0(\Omega.m)$		701.12	
Grain 1: Pyrite		Grain 2: Chalcopyrite	
Ellipticity e_1 (-)	1.11	Ellipticity e_2 (-)	9.63
Time Constant $\tau_1(s)$	9.29	Time Constant $\tau_2(s)$	0.03
Relaxation coefficient C_1 (-)	0.35	Relaxation coefficient C_2 (-)	0.74
Fraction volume $f_1(\%)$	6.64	Fraction volume $f_2(\%)$	0.13

CHAPTER 5

CONCLUSIONS

The GEMTIP model can be used for studying the petrophysical characteristics of rocks by analyzing the complex resistivity (CR) curves and inverting them for GEMTIP model parameters. However, the inversion of the CR data has proven to be very challenging due to the nonuniqueness and instability of this problem. In this thesis, I focused on the developing effective heuristic search methods for the inverse problem of the three-phase ellipsoidal GEMTIP model based on the genetic algorithms. GEMTIP forward modeling has been done to study the relationship between the GEMTIP parameters and the CR data.

The synthetic study showed that the pure genetic algorithm (GA) can be used to obtain the global minimum solution for the GEMTIP inversion. However, due to the precocity problem, this method only converged with some particular parameters setting. In order to improve inversion results, I have developed a novel hybrid adaptive genetic algorithm with simulated annealing (SAAGA) for the GEMTIP inversion. The synthetic study demonstrated that this method is not dependent on the setting of GA's parameters, and makes it possible to find the global minimum in the space of GEMTIP model parameters. However, in some rare situations when the observed CR curves of some rock samples are extremely complicated (e.g., weak local minimum the CR curve), the

SAAGA method may fail to converge to the global minimum solution. To solve this problem, I have proposed a modified hybrid genetic algorithm based on the SAAGA method and the three-point crossover operation.

In the case studies, first three mineral rock samples were examined by the three-phase ellipsoidal GEMTIP model using the SAAGA method. Complex resistivity data were provided by TechnoImaging. The quantitative values for the volume fractions obtained by the QEMSCAN system were used to constrain the inversion result. All the GEMTIP parameters were successfully recovered by the new method and were close to the inversion results predicted by the global minimum search (GMS) method, which proves that the SAAGA method provides an effective solution of GEMTIP inverse problem. Besides, two mineral rock samples were used to compare the SAAGA with multipoint crossover operation with the GMS method and the SAAGA method. While the inversion result of the SAAGA method failed to converge and the GMS method used several hours to obtain a local minimum solution, the modified method reached an extremely low misfit and obtained the global minimum solution within a few minutes. Thus, this method could be used as an alternative scheme for the inverse problem of the three-phase ellipsoidal GEMTIP model.

REFERENCES

Brown, D., C. Huntley, and A. Spillane, 1989, A parallel genetic heuristic for the quadratic assignment problem: Proceedings of 3rd International Conference on Genetic Algorithm, 406-415.

Burtman, V., A. V. Gribenko, and M. S. Zhdanov, 2010, Advances in experimental research of induced polarization effect in reservoir rocks: 80th Annual International Meeting, SEG, Expanded Abstracts, 2475–2479.

Burtman, V., M. Endo, M. S. Zhdanov, and T. Ingeman-Nielsen, 2011, High-frequency induced polarization measurements of hydrocarbon-bearing rocks: 81st Annual International Meeting, SEG, Expanded Abstracts, 677–681.

Cole, K. S., and R. H. Cole, 1941, Dispersion and absorption in dielectrics: Journal of Chemistry and Physics, **9**, 343-351.

Corana, A., M. Marchesi, C. Martini, and S. Ridella, 1987, Minimizing multimodal functions of continuous variables with the 'Simulated Annealing' Algorithm: ACM Transactions on Mathematical Software, **13**(3), 262-280.

Emond, A., M. S. Zhdanov, and E. U. Petersen, 2006, Electromagnetic modeling based on the rock physics description of the true complexity of rocks: Applications to porphyry copper deposits: 76th Annual International Meeting, SEG, Expanded Abstracts, 1313-1317a.

Emond, A. M., 2007, Electromagnetic modeling of porphyry systems from the grain-scale to the deposit-scale using the generalized effective medium theory of induced polarization: M. S. thesis, The University of Utah.

Fu, H., 2013, Interpretation of complex resistivity of the rocks using GEMTIP analysis: M. S. thesis, The University of Utah.

Gallard, R. H., and Esquivel, S. C., 2001, Enhancing evolutionary algorithms through recombination and parallelism: Journal of Computer Science and Technology, **1**.

Goffe, W. L., G. Ferrier, and J. Rogers, 1994, Global optimization of statistical functions with simulated annealing: Journal of Econometrics, **60**(1), 65-99.

Goldberg, D. E., 1989, Genetic Algorithms in search, optimization, and machine learning,

New York: Addison-Wesley.

Hammersley, J. M., and D. C. Handscomb, 1964, Monte Carlo Methods, London: Chapman & Hall.

Holland, J. H., 1975, Adaptation in natural and artificial systems, Ann Arbor: University of Michigan Press.

Kearey, P., M. Brooks, and I. Hill, 2009, An Introduction to Geophysical Exploration: John Wiley & Sons.

Kiberu, J., 2002, Induced polarization and resistivity measurements on a suite of near surface soil samples and their empirical relationship to selected measured engineering parameters: M. S. thesis, International Institute for Geo-information Science and Earth Observation, Enschede, The Netherlands.

Kirkpatrick, S. C., D. Gelatt, and M. P. Vecchi, 1983, Optimization by simulated annealing: Science, **220**, 671-680.

Lin, W., 2012, The application of 3D inversion of gravity anomaly with GPU parallel computing in the Nansha Area of South China Sea: M.S. thesis, Graduate University of Chinese Academy of Sciences.

Luo, Y., and G. Zhang, 1998, Theory and application of spectral induced polarization: Society of Exploration Geophysicists, Tulsa, OK.

Nelson, P. H., 1997, Induced polarization research at Kennecott, 1965-1977: The Leading Edge, **16**, 29-33.

Ostrander, A. G., and K. L. Zonge, 1978, Complex resistivity measurements of sulfide-bearing synthetic rocks: 48th Annual International Meeting, SEG, Expanded Abstracts.

Parasnis, D. S., 1973, Mining Geophysics: Elsevier Publishing Company, Amsterdam London New York.

Parker, P. B., 1999, Genetic algorithms and their use in geophysical problems: Ph.D. thesis, University of California at Berkeley.

Pelton, W. H., 1977, Interpretation of induced polarization and resistivity data: Ph.D. thesis, The University of Utah.

Pelton, W. H., S. H. Ward, P. G. Hallof, W. R. Sills, and P. H. Nelson, 1978, Mineral discrimination and removal of inductive coupling with multifrequency IP: Geophysics, **43**, 588-609.

Phillips, C. R., 2010, Experimental study of the induced polarization effect using Cole-Cole and GEMTIP models: Ph.D. thesis, The University of Utah.

Reynolds, J. M., 1997, An introduction to applied and environmental geophysics: Wiley

Sen, M. K., and P. L. Stoffa, 1992, Rapid sampling of model space using genetic algorithms: examples from seismic waveform inversion: Geophysical Journal International, **108**(1), 281-292.

Seigel, H., M. Nabighian, D. S. Parasnis, and K. Vozoff, 2007, The early history of the induced polarization method: The Leading Edge, **26**, 312-321.

Sliwinski, J., M. Power, P. Hughes, and J. Harrington, 2010, Integrated Shale Gas Evaluation: A study of QEMSCAN, SEM and Optical Petrography, XRD and Geochemistry of selected potential and producing North American Gas Shales: GeoCanada 2010.

Spears, W. M., and K. A. De Jong, 1990, An analysis of multipoint crossover: NAVAL RESEARCH LAB WASHINGTON DC.

Srinivas, M., and L. Patnaik, 2002, Adaptive probabilities of crossover and mutation in genetic algorithms: Systems, Man and Cybernetics, IEEE Transactions on Systems Man and Cybernetics, **24**(4), 656-667.

Sumner, J. S., 1976, Principles of induced polarization for geophysical exploration: Elsevier.

Telford, W. M., Geldart, L. P., Sheriff, R. E., and Keys, D. S., 1976, Applied geophysics: Cambridge University Press.

Vanhala, H., 1997, Mapping oil-contaminated sand and till with the spectral induced polarization (SIP) method, Geophysical Prospecting, **45**, 303-326.

Zhdanov, M. S., 2002, Geophysical inverse theory and regularization problems: Elsevier, Amsterdam.

Zhdanov, M. S., 2008, Generalized effective-medium theory of induced polarization: Geophysics, **73**, 197-211.

Zhdanov, M. S., 2009, Geophysical electromagnetic theory and methods: Elsevier, Amsterdam.

Zhdanov, M. S., V. Burtman, and A. Gribenko, 2009, Analysis of isotropic and anisotropic IP response of rocks based on the generalized effective-medium theory: Proceedings of the Annual Meeting of the Consortium for Electromagnetic Modeling and Inversion, The University of Utah, 71-96.

Zonge, K. L., W. A. Sauck, and J. S. Sumner, 1971, Comparison of time, frequency, and phase measurements in induced polarization: Geophysical Prospecting, **20**, 626-648.